Self-Similarities and Power-laws in the Time-resolved Spectra of

GRB 190114C, 130427A, 160509A, and 160625B

Liang Li

Co-authors: R. Ruffini, R. Moradi, J. A. Rueda, Yu Wang, S. S. Xue

ICRANet

ICRANet - Isfahan Astronomy Meeting, November 3rd 2021

- *Self-similarity and power-laws in GRB 190114C (arXiv:1904.04162)*
- *Self-Similarities and Power-laws in the Time-resolved Spectra of GRB 190114C, GRB 130427A, GRB 160509A, and GRB 160625B (arXiv:1910.12615)*
- *GRB-SNe association within Binary driven Hypernova (BdHN) (In prep.)*

SATELLITE

Neil Gehrels Swift Observatory

Swift is NASA space satellite. It is the first multi-wavelength observatory dedicated to the study of gamma-ray-burst (GRB) science. Its three instruments work together to observe GRBs and afterglows in the gamma-ray (Burst Alert Telescope, BAT), X-ray (X-ray Telescope, XRT), ultraviolet, and optical wavebands (Ultraviolet/ Optical Telescope, UVOT). Swift monitors the sky for new GRBs with a wide-field detector, localizes their positions onboard, and autonomously reorients itself to observe the new burst quickly with its other telescopes.

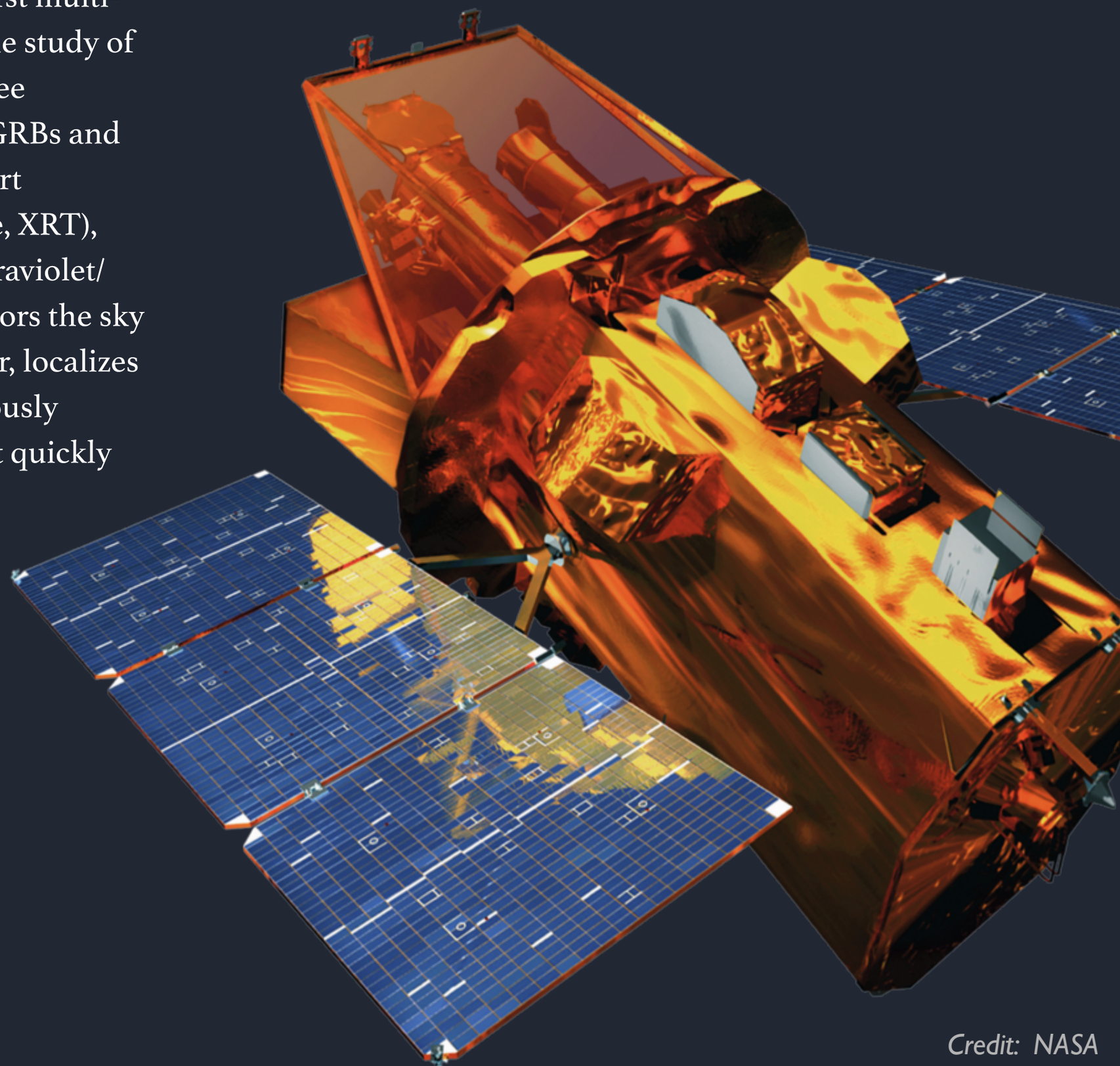

Credit: NASA

SATELLITE

Fermi Gamma-ray Space Telescope

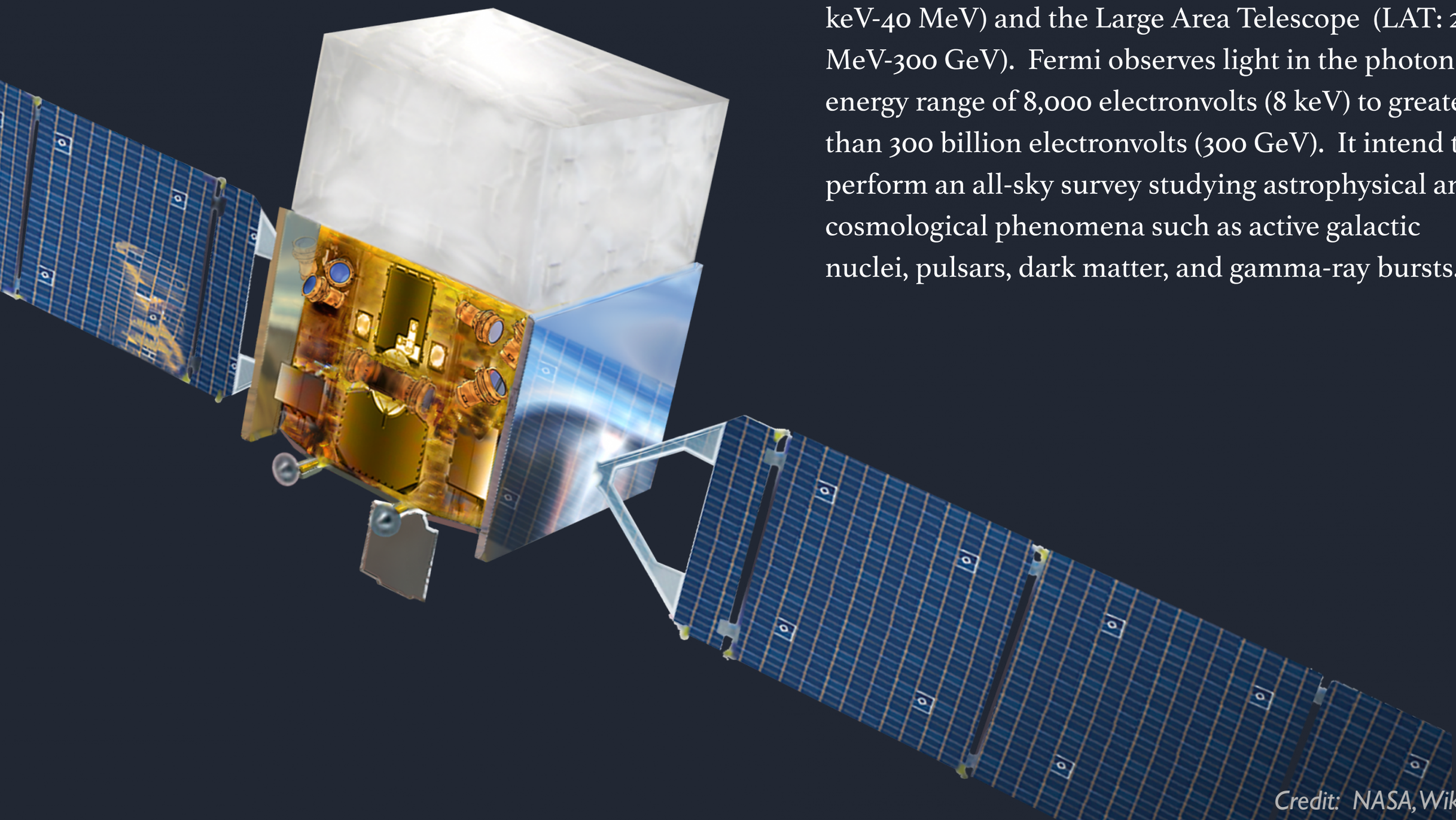

The Fermi Gamma-ray Space Telescope is a NASA space observatory being used to perform gamma-ray astronomy observations from low Earth orbit. Two instruments: the Gamma-ray Burst Monitor (GBM: 8 keV-40 MeV) and the Large Area Telescope (LAT: 20 MeV-300 GeV). Fermi observes light in the photon energy range of 8,000 electronvolts (8 keV) to greater than 300 billion electronvolts (300 GeV). It intend to perform an all-sky survey studying astrophysical and cosmological phenomena such as active galactic nuclei, pulsars, dark matter, and gamma-ray bursts.

Credit: NASA, Wikipedia

TELESCOPE

Major Atmospheric Gamma Imaging Cherenkov telescope (MAGIC)

MAGIC (Major Atmospheric Gamma Imaging Cherenkov Telescopes) is a system of two Imaging Atmospheric Cherenkov telescopes situated at the Roque de los Muchachos Observatory on La Palma, one of the Canary Islands, at about 2200 m above sea level. MAGIC is a system of two 17m diameter, F/1.03 Imaging Atmospheric Cherenkov Telescopes (IACT). They are dedicated to the observation of gamma rays from galactic and extragalactic sources in the very high energy range (VHE, 30 GeV to 100 TeV).

Credit: Max Planck Institue, Wikipedia

The best model of time-resolved spectral fit for GRB 110721A: Band+Blackbody

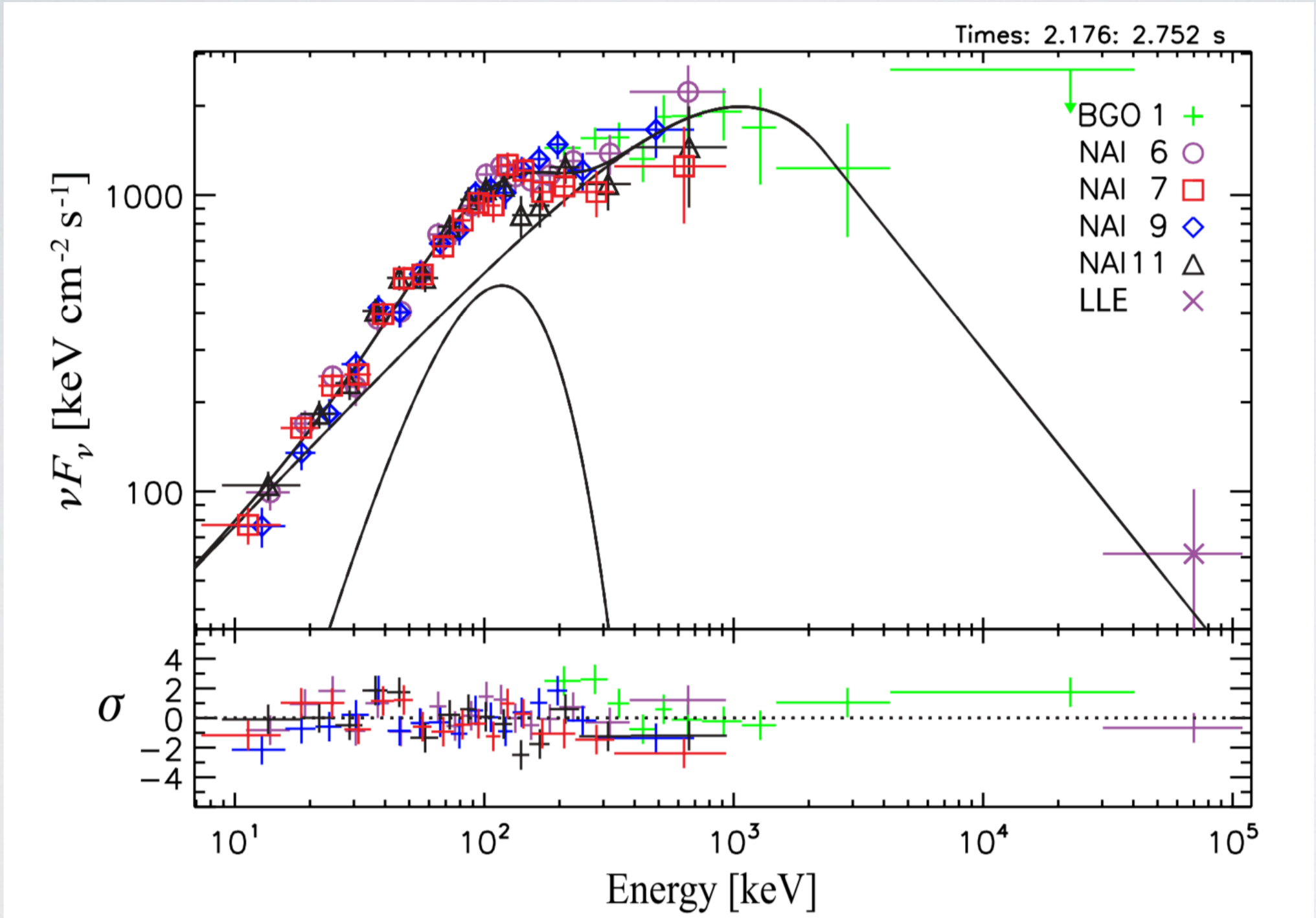

Figure is taken from Iyyani, S et al. (2015), MNRAS, 450, 1651

Synchrotron (non-thermal) & Photosphere (thermal)

The Definition of models

The Band function (Band et al. 1993) is defined as

$$f_{\rm BAND}(E) = A \begin{cases} (\frac{E}{E_{\rm piv}})^{\alpha} \exp(-\frac{E}{E_0}), & E \leq (\alpha-\beta)E_0 \\ [\frac{(\alpha-\beta)E_0}{E_{\rm piv}}]^{(\alpha-\beta)} \exp(\beta-\alpha)(\frac{E}{E_{\rm piv}})^{\beta}, & E \geq (\alpha-\beta)E_0 \end{cases} \quad \text{(A1)}$$

where

$$E_{\rm p} = (2+\alpha)E_0, \quad \text{(A2)}$$

where A is the normalization factor at 100 keV in units of ph cm^{-2}keV^{-1}s^{-1}, $E_{\rm piv}$ is the pivot energy fixed at 100 keV, α and β are the low-energy and high-energy power-law photon spectral indices, respectively. The two spectral regimes are separated by the break energy E_0 in units of keV, and $E_{\rm p}$ is the peak energy in the νF_ν space in units of keV.

The cutoff power law, or the so-called Comptonized model (COMP), which is written as

$$f_{\rm COMP}(E) = A \left(\frac{E}{E_{\rm piv}}\right)^{\alpha} e^{-E/E_0} \quad \text{(A3)}$$

The blackbody emission (BB) can be modified by Planck spectrum, which is given by the photon flux

$$f_{\rm BB}(E,t) = A(t) \frac{E^2}{\exp[\frac{E}{kT(\rm t)}] - 1}, \quad \text{(A4)}$$

where E is the photon energy, k is the Boltzmann constant. The blackbody emission depends on two free parameters only: temperature, $T(\rm t)$, and the normalisation, $A(\rm t)$.

Equations are taken from Li, et al. (2020), ApJ, 894, 100

Typical values for these model parameters from Fermi observations:

α ~ -1.0; β ~ -2.2 ; Ep ~ 250 keV; kT: 30 kev ~150 keV

Parameter estimation (spectral fitting) using Bayesian inference+MCMC method

Bayes's theorem is applied to infer and update the probability distribution of a specific set of model parameters. For instance, given an observed data set (D) and a profile model (M), the probability distribution $p(M \mid D)$, i.e., so-called *Posterior* probability, according to the Bayes's theorem, therefore is given by

$$p(M \mid D) = \frac{p(D \mid M)p(M)}{p(M)}, \tag{1}$$

where, $p(D \mid M)$ is the likelihood that combines the model and the observed data and expresses the probability to observe (or to generate) the data set D from given a model M with its parameters, $p(M)$ is prior on the model parameters, and $p(D)$ is called evidence, which is constant with the purpose of normalizing.

When using Bayesian posterior sampling, according to the Bayes's theorem, only the simplest posterior allows for an analytic solution. However, a high-dimensional integration is required in most cases so that the posterior is generally impossible to compute. Therefore stochastic sampling techniques such as MCMC or nested sampling methods are must be involved[4]. Two popular posterior

- *Package: the Multi-Mission Maximum Likelihood Framework (3ML).*

See Li. (2020), ApJ, 894, 100

Binary Driven Hypernova Type I

ICRANet **Remo Ruffini**
INAF *and ICRANet Collaboration*
Sapienza Universita di Roma
Universite de Nice Sophia Antipolis
University Campus Bio-Medico of Rome

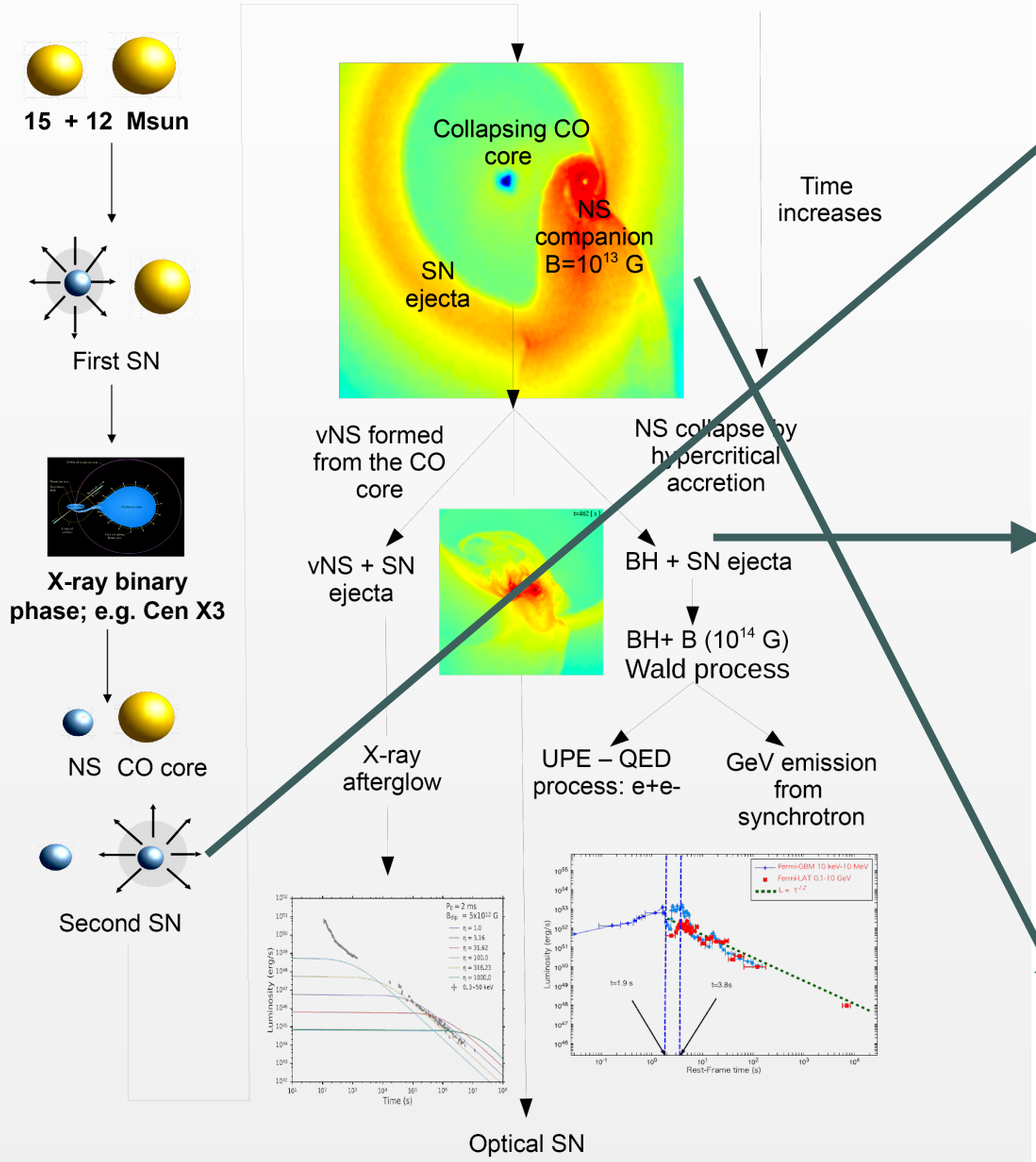

Schematic example of the evolutionary path of a massive binary all the way up to the formation of a BdHN I. The BdHN progenitor is a binary composed of a CO core and a magnetized (B~10^{13} G) NS companion in a very compact orbit (period of the order of minutes). To reach the BdHN stage the binary has to survive two SN events: the first SN forms the NS and the second one the νNS (core-collapse of the COcore). The SN ejecta produce a massive and rapid accretion process onto the NS companion leading to its gravitational collapse forming a BH. Conservation of magnetic flux and possibly additional MHD processes amplify the magnetic field from the NS value to B~10^{14}G around the BH. While the SN matter expands, before escaping from the system it surrounds both the νNS and the BH. The B-field together with the BH rotation triggers the "Wald" process which induces an electric field. This E-field explains both the UPE in the gamma-rays through the transparency of the self-accelerating e−e+ pair plasma created by the QED process of vacuum breakdown, and the GeV emission through synchrotron emission of accelerated protons in the B-field. The interaction of the νNS pulsar emission with the SN ejecta explains the X-ray afterglow. Finally, after about 15 days, the optical emission of the SN produced by the energy release of the decay of Nickel, is observed.

- *The spectrum characteristic of the νNv-rise indicate a thermal component.*
- *The spectrum characteristic of the UPE phase also indicate a thermal component.*
- *The spectrum characteristic of the cavity should shows a featureless non-thermal component.*

- *Self-similarity and power-laws in GRB 190114C (arXiv:1904.04162)*
- *Self-Similarities and Power-laws in the Time-resolved Spectra of GRB 190114C, GRB 130427A, GRB 160509A, and GRB 160625B (arXiv:1910.12615)*
- *GRB-SNe association within Binary driven Hypernova (BdHN) (In prep.)*

Self-similarity and power-laws in GRB 190114C

Episode 1: precursor (vNv-rise and the creation of the new neutron star).

Episode 2: three major events: (1) the formation of the BH, (2) the onset of the GeV emission, and (3) the onset of the ultra-relativistic prompt emission (UPE).

Episode 3: the presence of a 'cavity' carved out in the SN ejecta by the BH formation.

See Ruffini R., et al. (2019), arXiv: 1904.04162

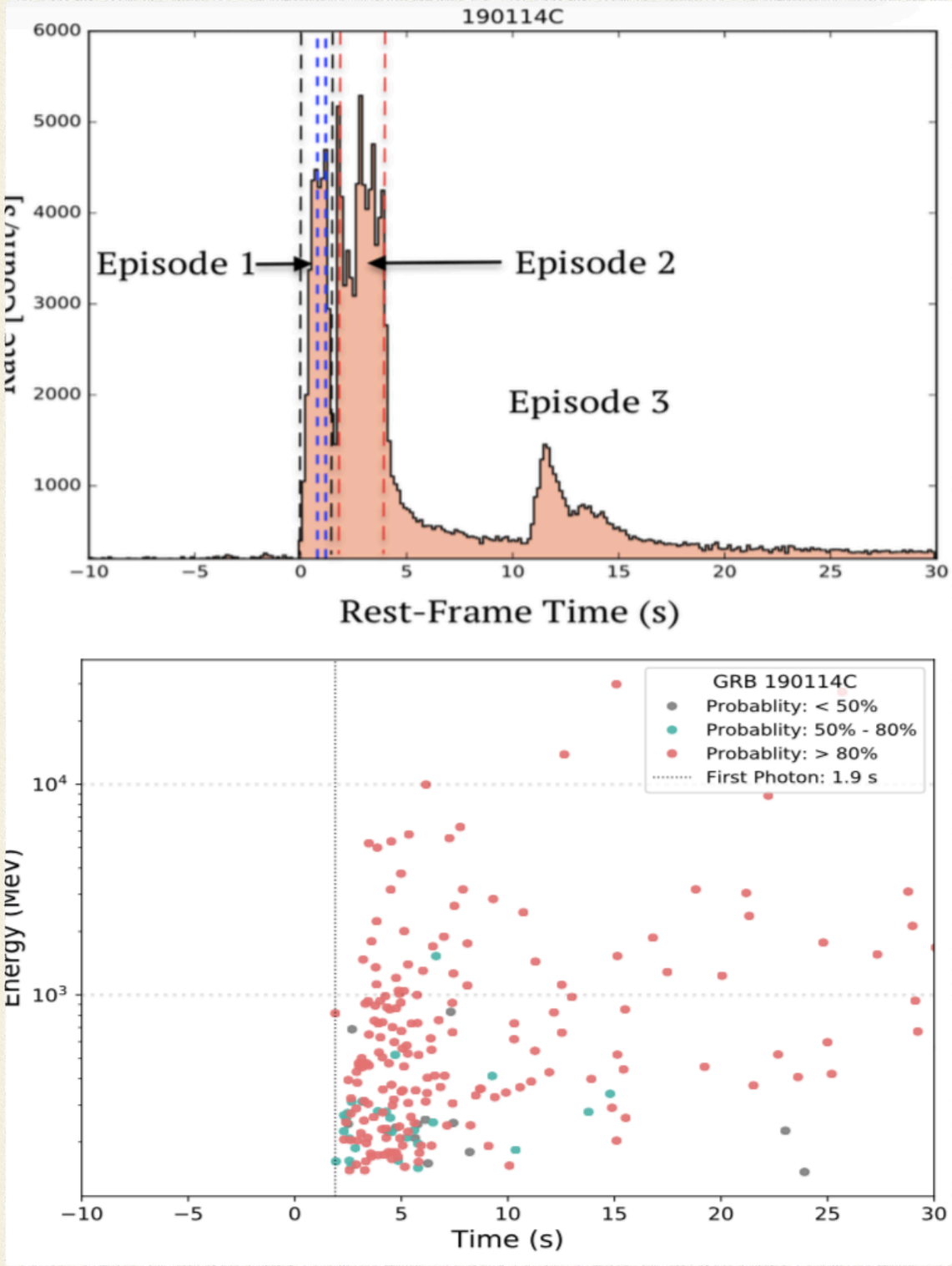

Self-similarity and power-laws in GRB 190114C

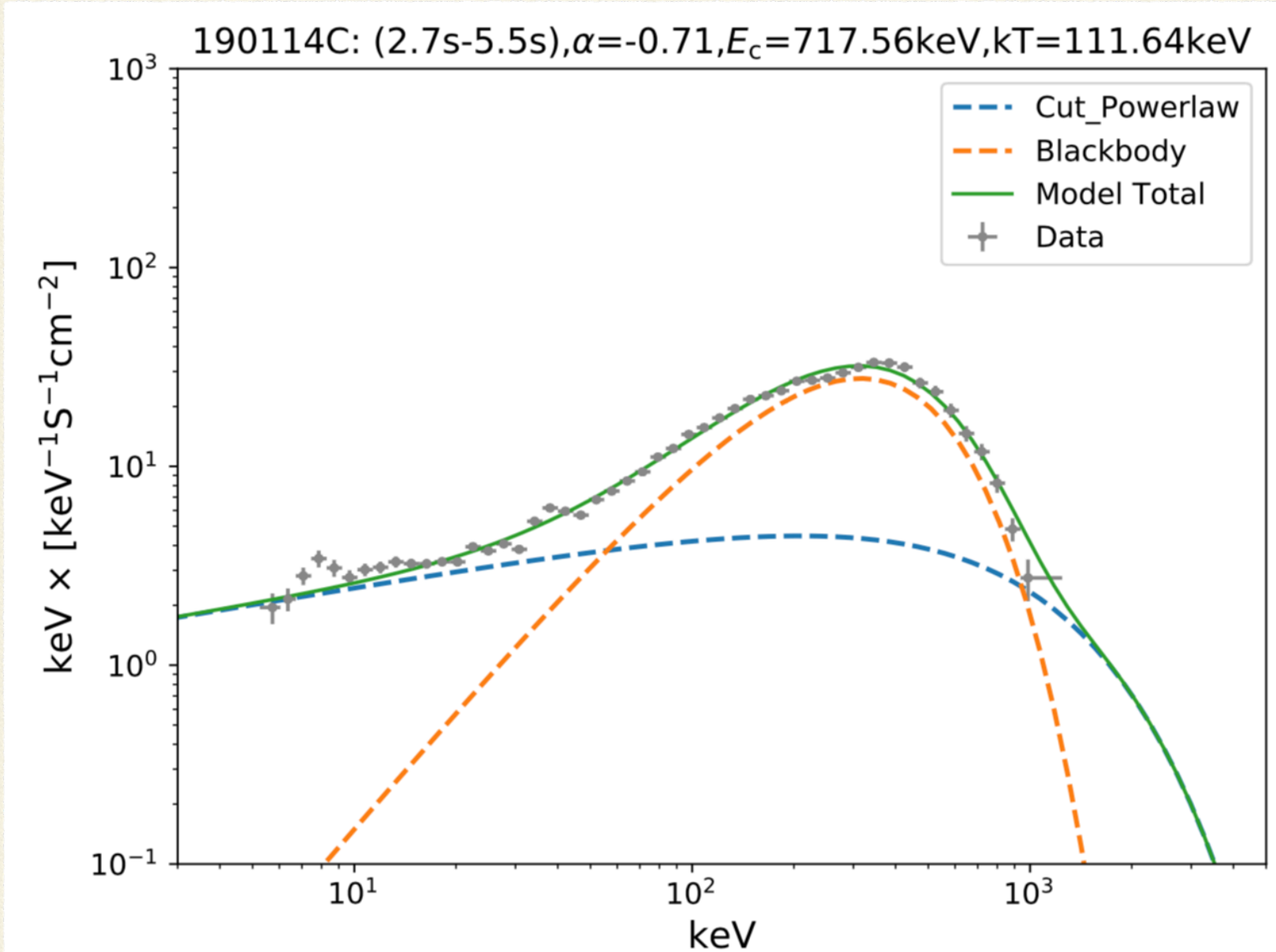

- *Model comparisons: the deviance formation criterion (DIC).*
  - *We perform the spectral analysis in 5 successive time iterations in increasingly shorter time bins: this is the first iteration for entire time interval for UPE (Episode II) .*

See Ruffini R., et al. (2019), arXiv: 1904.04162

Self-similarity and power-laws in GRB 190114C

5 successive time iterations for UPE (Episode II)

- Iteration 2: repetition Iteration 1 but with divided into two equal parts.
- Iteration 3: the same as Iteration 2 but for four equal parts.
- Iteration 4:the same as Iteration 2 but for eight equal parts.
- Iteration 5:the same as Iteration 2 but for sixteen equal parts.

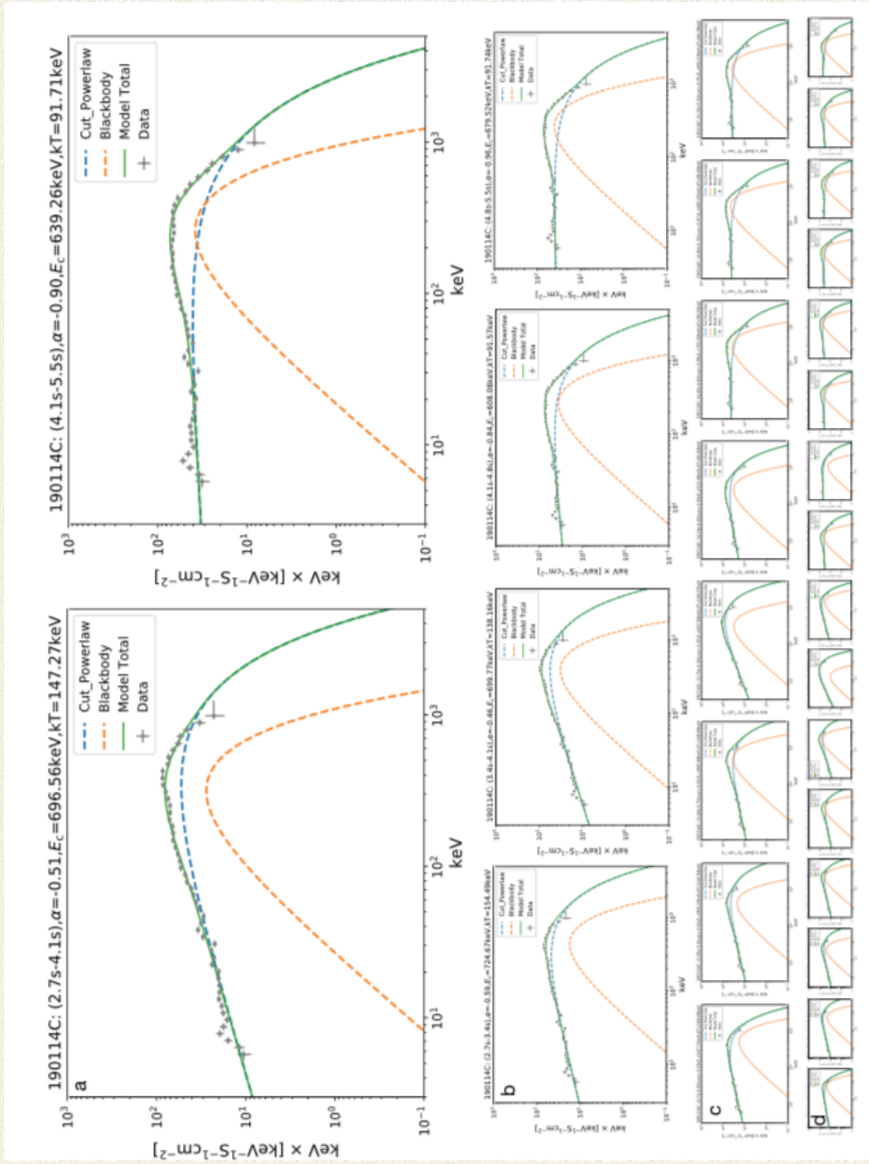

See Ruffini R., et al. (2019), arXiv: 1904.04162

We find a similarity in the spectra in each stage of the iterations revealing clearly a self-similar structure.

Self-similarity and power-laws in GRB 190114C

Table 2. Results of the time-resolved Spectral fits of GRB 190114C (CPL+BB model) from $t_{\rm rf}$ = 1.9 s to $t_{\rm rf}$ = 3.99 s. The time intervals both in the rest-frame and observer frame, the power-law index, cut-off energy, temperature, AIC/BIC, BB flux, total flux, the ratio of black body flux to the total flux, $F_{\rm BB}/F_{\rm Total}$ and finally the isotropic energy are reported in this table. The $F_{\rm BB}/F_{\rm Total}$ remains almost constant in each sample. The Akaike Information Criterion (AIC, Akaike 1974) and the Bayesian Information Criterion (BIC, Schwarz et al. 1978) can be used to select non-nested models. The AIC and BIC are defined as AIC=-2ln$L(\vec{\theta})$+2k and BIC=-2ln$L(\vec{\theta})$+kln(n), respectively. Here L is the maximized value of the likelihood function for the estimated model, k is the number of free parameters to be estimated, n is the number of observations (or the sample size). The prefer model between any two estimated models is the one that provides the minimum AIC and BIC scores. After comparing the AIC and BIC , we find the CPL+BB model is the preferred model than the CPL and other model. The likelihood -log(posterior) and the AIC and BIC scores are reported in column 6. There is in the fifth iteration a delay of 0.1 s between the onset of the GeV radiation and the onset of the UPE.

t_1~t_2	t_1~t_2	α	E_c	kT	-log(posterior)/(AIC/BIC)	$F_{\rm BB}$	$F_{\rm Total}$	$F_{\rm ratio}$	$E_{\rm Total}$
(s) Observation	(s) Rest		(keV)	(keV) Rest		(10^{-6}) (erg cm^{-2} s^{-1})	(10^{-6}) (erg cm^{-2} s^{-1})		(erg) Rest
(1)	(2)	(3)	(4)	(5)	(6)	(7)	(8)	(9)	(10)
2.700~5.500	1.896~3.862	$-0.71^{+0.02}_{-0.02}$	$717.6^{+25.4}_{-25.4}$	$159.0^{+3.6}_{-3.6}$	-3344/6697/6719	$22.49^{+3.21}_{-2.65}$	$111.10^{+11.60}_{-10.40}$	0.20	1.50e+53
2.700~4.100	1.896~2.879	$-0.51^{+0.02}_{-0.02}$	$696.6^{+31.9}_{-32.4}$	$209.7^{+9.3}_{-9.1}$	-2675/5360/5381	$24.67^{+6.93}_{-5.35}$	$142.50^{+23.90}_{-21.00}$	0.17	9.64e+52
4.100~5.500	2.879~3.862	$-0.90^{+0.02}_{-0.02}$	$639.3^{+31.9}_{-31.6}$	$130.6^{+2.5}_{-2.5}$	-2529/5069/5090	$25.55^{+2.97}_{-2.75}$	$80.98^{+9.68}_{-8.07}$	0.32	5.48e+52
2.700~3.400	1.896~2.388	$-0.59^{+0.03}_{-0.03}$	$724.7^{+44.5}_{-45.5}$	$220.0^{+17.1}_{-17.2}$	-1882/3774/3796	$18.55^{+9.42}_{-7.40}$	$123.90^{+29.20}_{-22.30}$	0.15	4.19e+52
3.400~4.100	2.388~2.879	$-0.46^{+0.04}_{-0.04}$	$699.8^{+47.8}_{-48.3}$	$196.7^{+8.9}_{-8.7}$	-2032/4074/4095	$31.78^{+9.60}_{-7.31}$	$161.40^{+47.10}_{-32.40}$	0.20	5.46e+52
4.100~4.800	2.879~3.371	$-0.84^{+0.03}_{-0.03}$	$608.1^{+42.1}_{-42.2}$	$130.4^{+3.7}_{-3.9}$	-1880/3770/3792	$23.94^{+4.20}_{-4.22}$	$85.37^{+14.83}_{-12.27}$	0.28	2.89e+52
4.800~5.500	3.371~3.862	$-0.96^{+0.03}_{-0.03}$	$679.5^{+49.1}_{-48.7}$	$130.6^{+3.1}_{-3.2}$	-1809/3628/3649	$27.18^{+4.01}_{-3.73}$	$78.20^{+11.40}_{-9.66}$	0.35	2.65e+52
2.700~3.050	1.896~2.142	$-0.59^{+0.03}_{-0.03}$	$547.7^{+44.2}_{-44.9}$	$240.8^{+29.2}_{-29.1}$	-1187/2384/2406	$19.67^{+17.96}_{-8.88}$	$103.20^{+30.60}_{-20.28}$	0.19	1.75e+52
3.050~3.400	2.142~2.388	$-0.60^{+0.02}_{-0.02}$	$965.2^{+28.5}_{-30.1}$	$203.5^{+14.8}_{-14.8}$	-1320/2650/2671	$22.87^{+8.88}_{-7.23}$	$152.00^{+24.00}_{-21.00}$	0.15	2.57e+52
3.400~3.750	2.388~2.633	$-0.63^{+0.04}_{-0.04}$	$885.7^{+70.9}_{-70.1}$	$240.6^{+10.5}_{-10.6}$	-1224/2458/2480	$41.02^{+11.09}_{-7.91}$	$129.10^{+32.40}_{-23.40}$	0.32	2.18e+52
3.750~4.100	2.633~2.879	$-0.35^{+0.06}_{-0.05}$	$607.8^{+57.1}_{-60.1}$	$151.5^{+12.4}_{-14.2}$	-1428/2866/2887	$23.92^{+12.46}_{-10.40}$	$192.00^{+101.70}_{-60.30}$	0.12	3.25e+52
4.100~4.450	2.879~3.125	$-0.69^{+0.04}_{-0.04}$	$515.9^{+43.6}_{-43.6}$	$117.3^{+5.0}_{-5.0}$	-1271/2552/2573	$19.19^{+4.89}_{-4.40}$	$92.71^{+27.69}_{-22.43}$	0.21	1.57e+52
4.450~4.800	3.125~3.371	$-0.98^{+0.04}_{-0.04}$	$702.0^{+78.1}_{-78.2}$	$141.3^{+5.8}_{-5.8}$	-1254/2518/2539	$26.76^{+6.41}_{-5.47}$	$80.73^{+17.95}_{-14.95}$	0.33	1.37e+52
4.800~5.150	3.371~3.617	$-0.97^{+0.04}_{-0.04}$	$685.1^{+69.4}_{-68.6}$	$140.8^{+4.6}_{-4.6}$	-1218/2447/2468	$31.83^{+6.85}_{-4.98}$	$82.51^{+15.62}_{-12.33}$	0.39	1.40e+52
5.150~5.500	3.617~3.862	$-0.95^{+0.04}_{-0.04}$	$692.2^{+79.1}_{-77.7}$	$120.0^{+4.0}_{-4.0}$	-1203/2416/2438	$23.19^{+5.38}_{-3.81}$	$73.57^{+18.69}_{-12.93}$	0.32	1.24e+52
2.875~3.050	2.019~2.142	$-0.68^{+0.04}_{-0.05}$	$627.6^{+87.0}_{-91.5}$	$258.0^{+30.1}_{-28.7}$	-664/1337/1359	$28.45^{+20.42}_{-12.51}$	$98.14^{+33.56}_{-26.44}$	0.29	8.30e+51
3.050~3.225	2.142~2.265	$-0.59^{+0.03}_{-0.03}$	$957.1^{+34.1}_{-34.9}$	$245.3^{+21.5}_{-21.0}$	-768/1547/1568	$25.71^{+13.87}_{-9.03}$	$169.30^{+38.20}_{-31.60}$	0.15	1.43e+52
3.225~3.400	2.265~2.388	$-0.59^{+0.03}_{-0.03}$	$929.6^{+55.7}_{-58.7}$	$172.4^{+15.8}_{-15.8}$	-759/1527/1549	$20.60^{+11.17}_{-8.22}$	$136.00^{+37.90}_{-26.70}$	0.15	1.15e+52
3.400~3.575	2.388~2.511	$-0.59^{+0.05}_{-0.05}$	$804.0^{+86.7}_{-82.3}$	$255.9^{+17.4}_{-17.4}$	-702/1414/1436	$42.19^{+19.41}_{-13.59}$	$139.30^{+48.30}_{-35.60}$	0.30	1.18e+52
3.575~3.750	2.511~2.633	$-0.65^{+0.04}_{-0.04}$	$916.3^{+64.6}_{-67.7}$	$229.3^{+13.6}_{-13.5}$	-730/1471/1492	$39.25^{+11.97}_{-10.71}$	$119.50^{+32.90}_{-25.45}$	0.33	1.01e+52
3.750~3.925	2.633~2.756	$-0.51^{+0.02}_{-0.02}$	$960.9^{+30.9}_{-31.4}$	$204.6^{+9.9}_{-10.0}$	-808/1627/1648	$57.70^{+15.81}_{-12.25}$	$221.10^{+35.60}_{-31.50}$	0.26	1.87e+52
3.925~4.100	2.756~2.879	$-0.19^{+0.04}_{-0.04}$	$416.6^{+26.0}_{-26.3}$	$77.5^{+20.7}_{-16.1}$	-818/1646/1668	$4.29^{+6.85}_{-3.22}$	$177.30^{+57.10}_{-45.70}$	0.02	1.50e+52
4.100~4.275	2.879~3.002	$-0.54^{+0.06}_{-0.06}$	$474.1^{+45.5}_{-46.2}$	$162.6^{+14.9}_{-14.8}$	-758/1526/1547	$24.26^{+17.09}_{-10.09}$	$116.10^{+52.40}_{-35.12}$	0.21	9.82e+51
4.275~4.450	3.002~3.125	$-0.90^{+0.06}_{-0.06}$	$586.4^{+86.7}_{-89.0}$	$96.0^{+3.5}_{-3.5}$	-738/1485/1507	$21.95^{+4.75}_{-4.49}$	$70.69^{+29.51}_{-17.13}$	0.31	5.98e+51
4.450~4.625	3.125~3.248	$-0.96^{+0.20}_{-0.10}$	$679.6^{+148.4}_{-182.5}$	$107.9^{+33.0}_{-94.9}$	-722/1454/1475	$16.62^{+12.12}_{-16.62}$	$68.87^{+100.23}_{-28.45}$	0.24	5.82e+51
4.625~4.800	3.248~3.371	$-0.95^{+0.05}_{-0.05}$	$694.2^{+96.8}_{-94.2}$	$146.3^{+6.7}_{-6.6}$	-734/1477/1499	$35.59^{+9.47}_{-8.00}$	$89.91^{+27.59}_{-18.82}$	0.40	7.60e+51
4.800~4.975	3.371~3.494	$-0.85^{+0.05}_{-0.05}$	$564.5^{+68.9}_{-71.9}$	$135.3^{+7.5}_{-7.6}$	-744/1498/1519	$30.78^{+11.12}_{-8.55}$	$96.58^{+31.02}_{-23.68}$	0.32	8.17e+51
4.975~5.150	3.494~3.617	$-1.10^{+0.04}_{-0.04}$	$820.5^{+115.0}_{-111.2}$	$149.7^{+5.9}_{-5.8}$	-683/1376/1398	$32.76^{+6.98}_{-5.92}$	$71.57^{+16.74}_{-11.99}$	0.46	6.05e+51
5.150~5.325	3.617~3.739	$-1.04^{+0.05}_{-0.05}$	$765.2^{+119.0}_{-115.8}$	$130.9^{+5.8}_{-5.8}$	-697/1404/1426	$26.14^{+7.02}_{-5.96}$	$66.70^{+20.48}_{-14.17}$	0.39	5.64e+51
5.325~5.500	3.739~3.862	$-0.88^{+0.06}_{-0.06}$	$635.3^{+88.7}_{-92.0}$	$108.9^{+5.3}_{-5.4}$	-736/1483/1504	$20.90^{+6.51}_{-5.15}$	$79.48^{+28.02}_{-21.03}$	0.26	6.72e+51
5.500~5.675	3.862~3.985	$-1.10^{+0.08}_{-0.08}$	$568.5^{+130.8}_{-125.4}$	$73.4^{+2.1}_{-2.1}$	-657/1324/1345	$16.08^{+2.77}_{-2.56}$	$43.59^{+19.37}_{-10.92}$	0.37	3.69e+51

Table 2 summarize the parameters of the fitting for UPE (Episode II).

See Ruffini R., et al. (2019), arXiv: 1904.04162

Self-similarity and power-laws in GRB 190114C

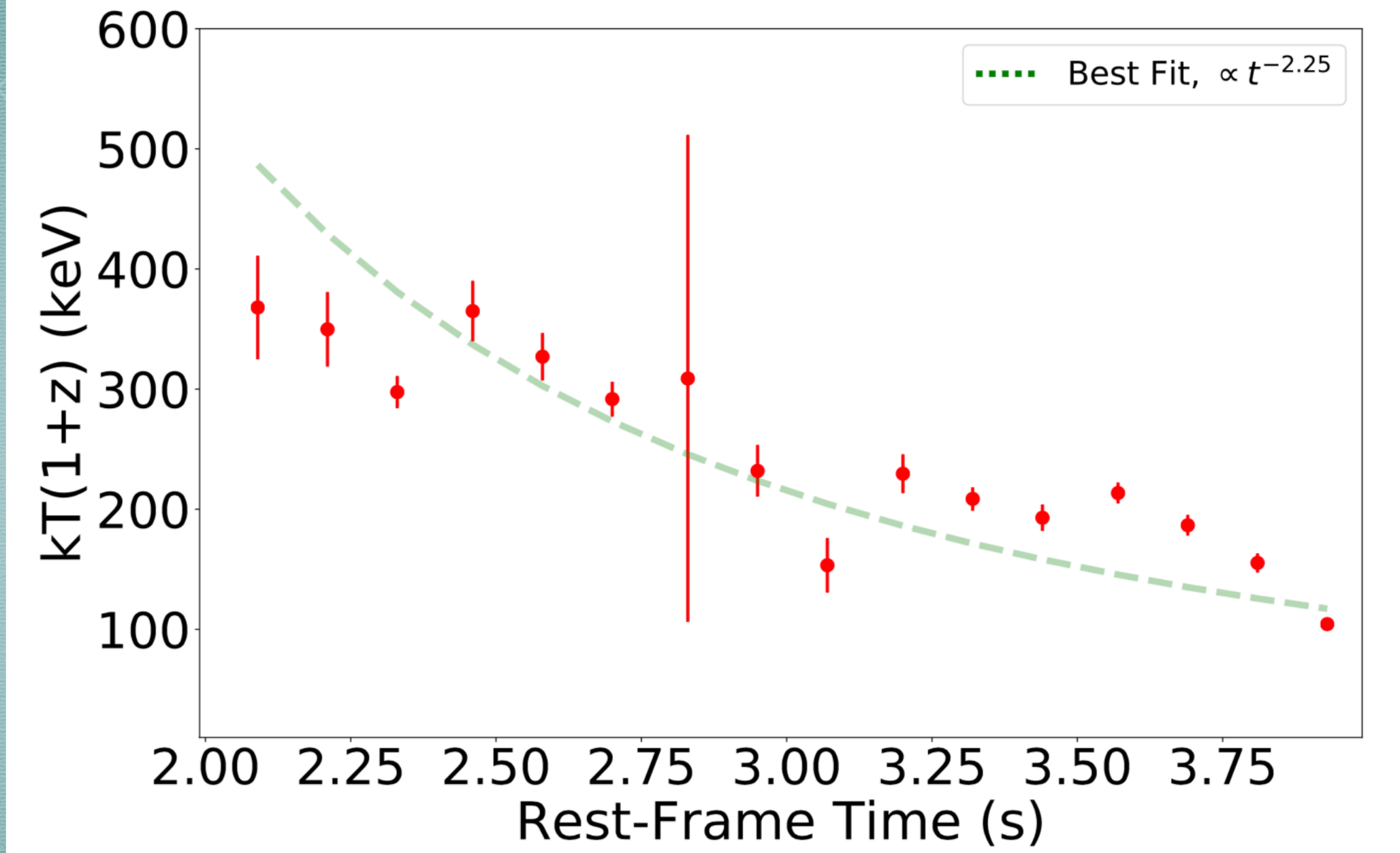

We find a power-law dependence of the BB temperature with index -2.25± 0.38.

See Ruffini R., et al. (2019), arXiv: 1904.04162

Self-similarity and power-laws in GRB 190114C

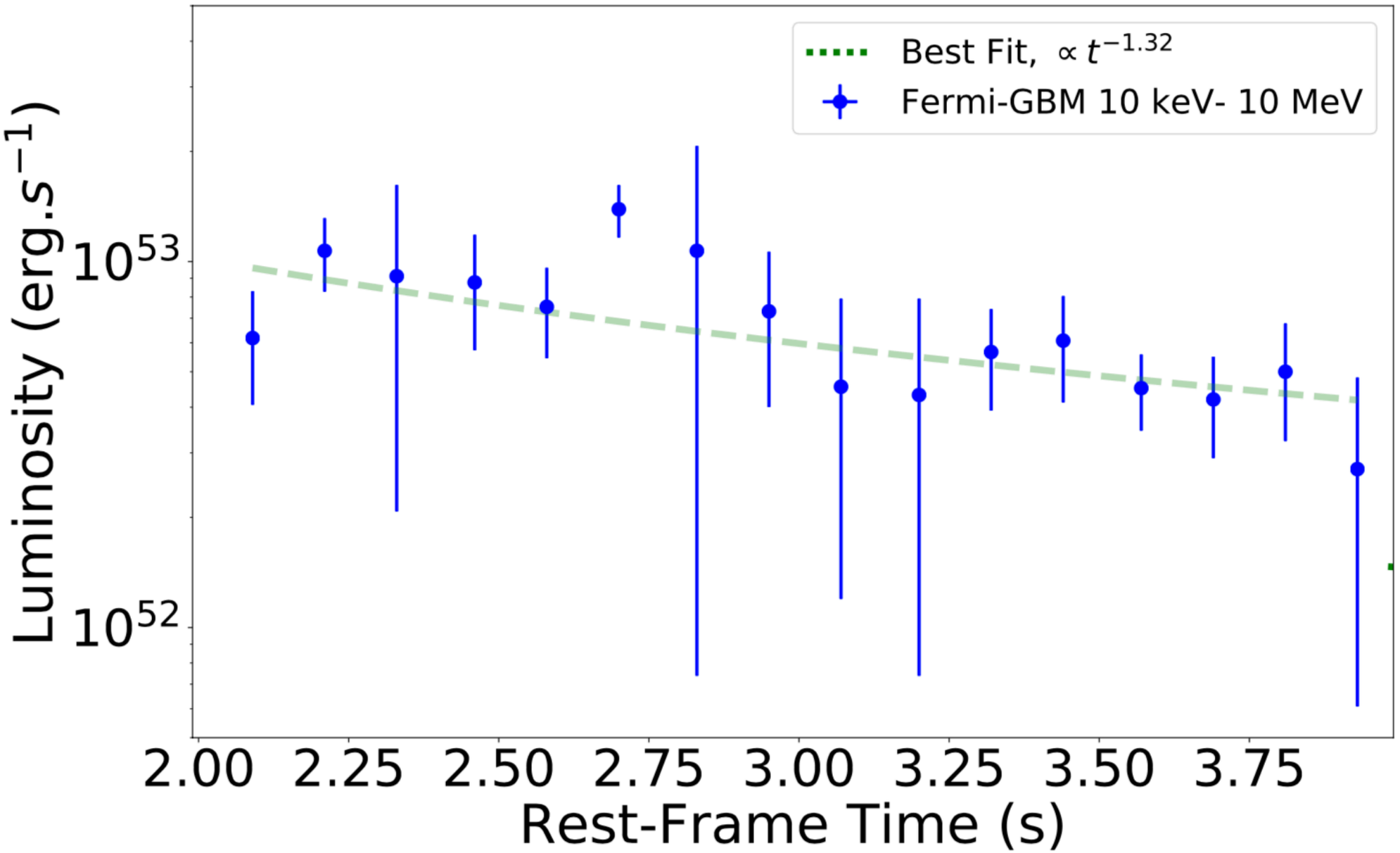

A dependence with index -1.32 ± 0.26 for the gamma-ray luminosity confirming a similar dependence with index -1.20 ± 0.36 which we find as well in the GeV luminosity, both expressed in the rest-frame.

See Ruffini R., et al. (2019), arXiv: 1904.04162

- *Self-similarity and power-laws in GRB 190114C (arXiv:1904.04162)*
- *Self-Similarities and Power-laws in the Time-resolved Spectra of GRB 190114C, GRB 130427A, GRB 160509A, and GRB 160625B (arXiv:1910.12615)*
- *GRB-SNe association within Binary driven Hypernova (BdHN) (In prep.)*

Self-Similarities and Power-laws in the Time-resolved Spectra of GRB 190114C, GRB 130427A, GRB 160509A, and GRB 160625B

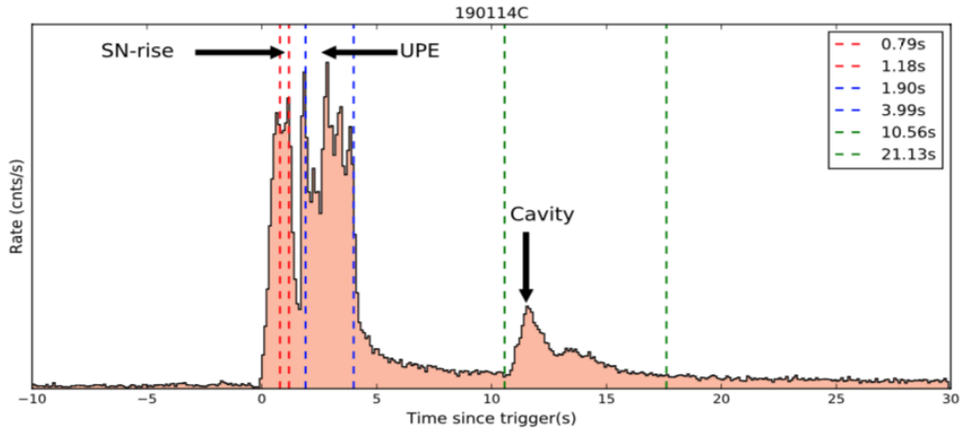

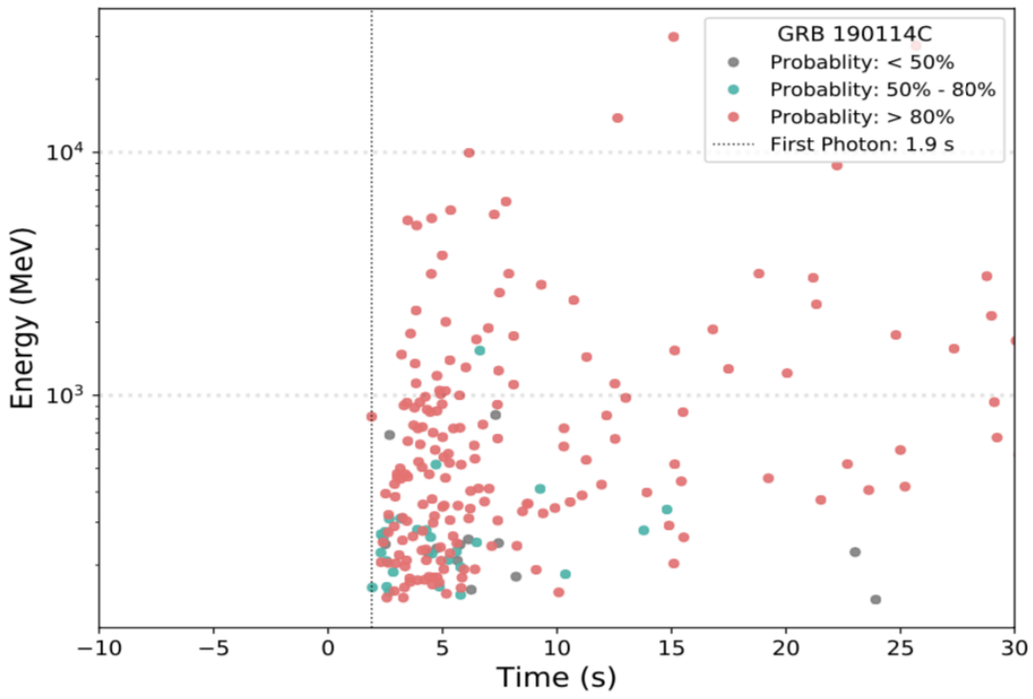

Figure 1. Top panel: the properties of the prompt emission of GRB 190114C in the rest frame. The redshift for GRB 190114C is 0.42 (Selsing et al. 2019a). The lightcurve consists of three spikes, the first one is Episode 1 (SN break out) with the energy $(2.82 \pm 0.13) \times 10^{52}$ erg, then we have Episode 2, the UPE phase, and then Episode 3, the emission from the cavity (Ruffini et al. 2019c). The total energy is $(2.48 \pm 0.20) \times 10^{53}$ erg (Wang et al. 2019a). Bottom panel: the onset of the Gev emission at the $t_{\rm rf} = 1.9$ s contestant with the turn-on of the Episode 2. Lower: the arrival time of Fermi-LAT photons in the energy band 0.1–100 GeV. The first photon of the UPE phase arrives at 1.9 s. The onset of the GeV radiation almost coincides with the onset of the UPE. The detailed information for each episode, as well as the GeV and afterglow emissions, see Section 3 and Table 1, which include the typical starting time, the duration, the isotropic energy, and the preferred model.

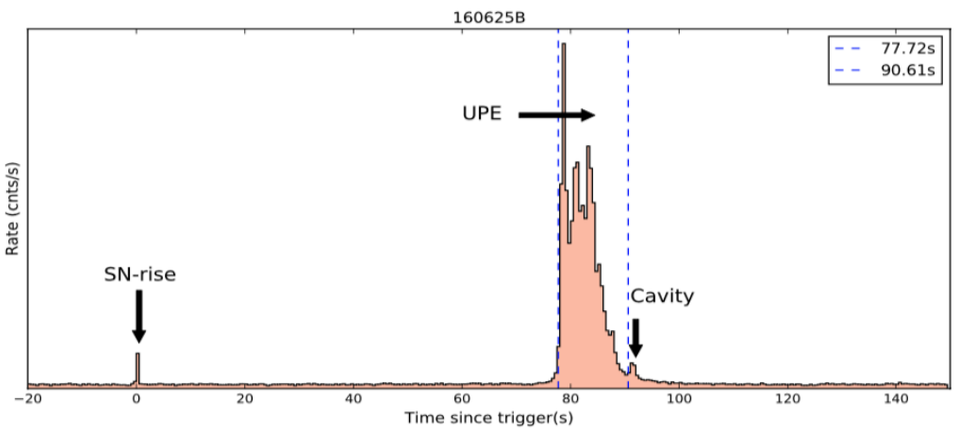

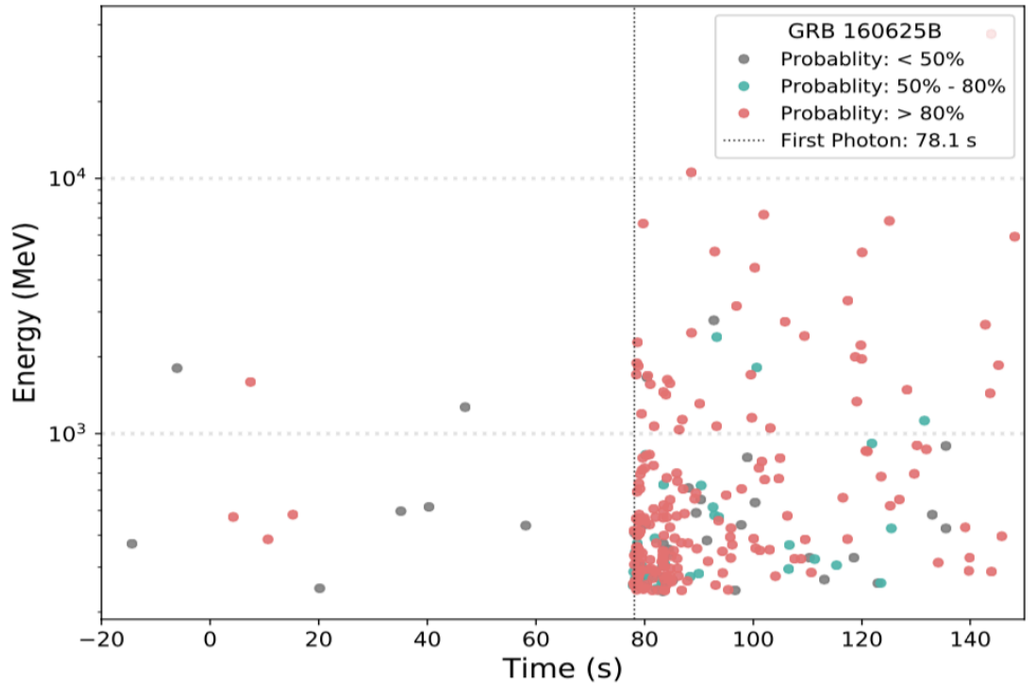

Figure 6. Upper panel: the proposed three new episodes of GRB 160625B as a function of the rest-frame time. Episode 1 occurs $t_{\rm rf} = 0$ s and $t_{\rm rf} = 0.83$ s. The blue dashed vertical lines represents the SN breakout. Episode 2 occurs from $t_{\rm rf} = 77.72$ s to $t_{\rm rf} = 86.03$ s, and includes the UPE emission. Episode 3 occurs at times after $t_{\rm rf} = 86.03$ s, staring at $t_{\rm rf} = 86.03$ s and ending at $t_{\rm rf} = 96.84$ s. The redshift for GRB 160625B is 1.406 (Xu et al. 2016). The light-curve consists of two clear spikes, the isotropic energy in the first one is $(1.09 \pm 0.20) \times 10^{52}$ erg. The total energy is $\approx 3 \times 10^{54}$ erg (Zhang et al. 2018). Lower panel: the arrival time of Fermi-LAT photons in the energy band 0.1–100 GeV. The first photon of the UPE phase arrives at 78.1 s. The onset of the GeV radiation almost coincides with the onset of the UPE. The detailed information for each episode, as well as the GeV and afterglow emissions, see Section 4 and Table 1, which include the typical starting time, the duration, the isotropic energy, and the preferred model.

Fermi-GBM light curves for our four sources, all four sources show three Episodes.

See Liang, L., et al. (2019), arXiv: 1910.12615

Self-Similarities and Power-laws in the Time-resolved Spectra of GRB 190114C, GRB 130427A, GRB 160509A, and GRB 160625B

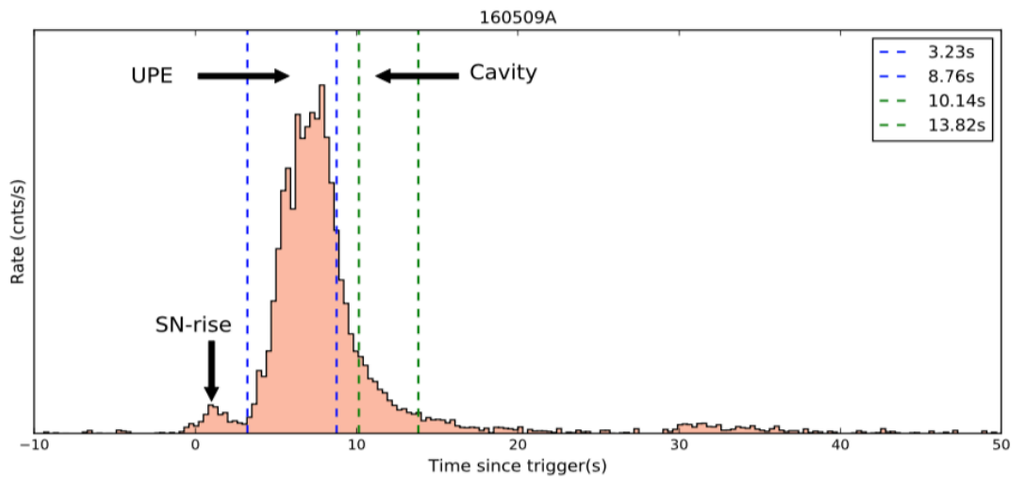

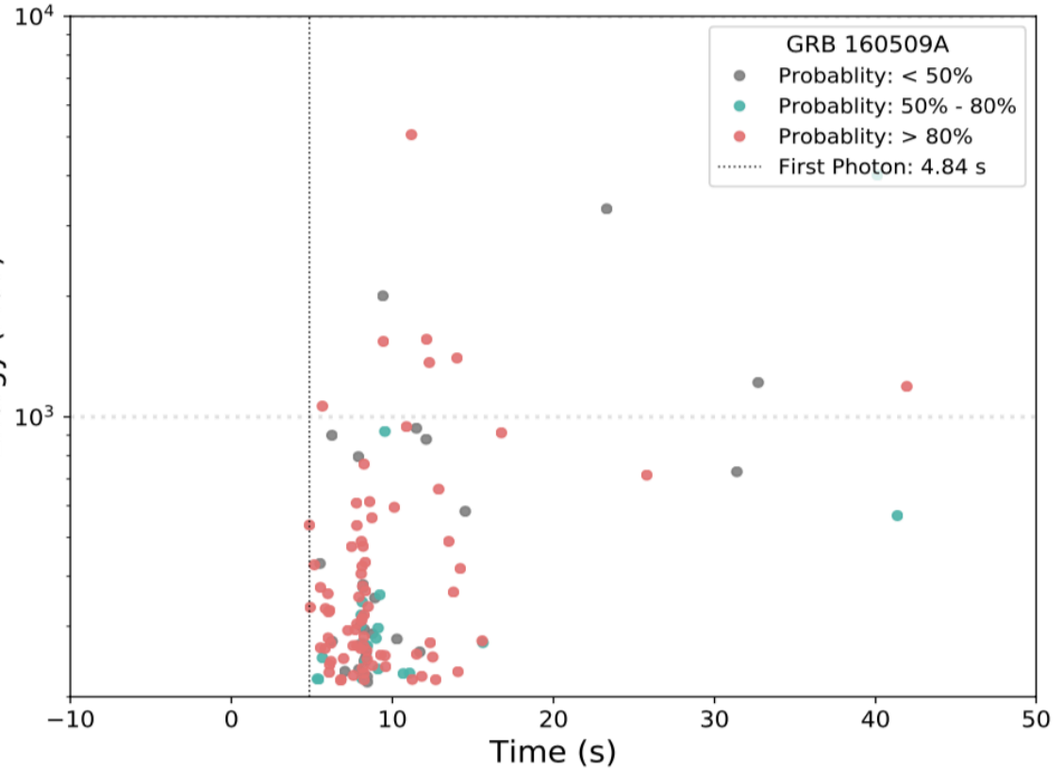

Figure 13. Upper panel: properties of the prompt emission phase of GRB 160509A. The redshift for GRB 160509A is 1.17 (Tanvir et al. 2016). The light-curve consists of two spikes, the isotropic energy in the first small one is $(2.96 \pm 0.60) \times 10^{52}$ erg. The total energy is 1.06×10^{54} erg (Tam et al. 2017). Lower panel: the arrival time of Fermi-LAT photons of energy > 100 MeV. The first photon of the UPE phase arrives at 4.84 s. The onset of the GeV radiation coincides with the onset of the UPE. The detailed information for each episode, as well as the GeV and afterglow emissions, see Section 5 and Table 1, which include the typical starting time, the duration, the isotropic energy, and the preferred model.

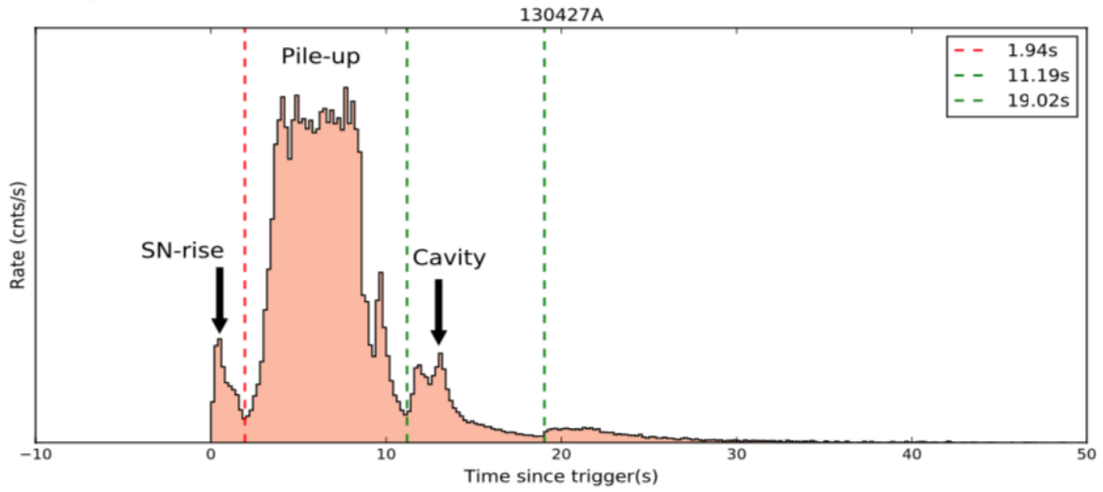

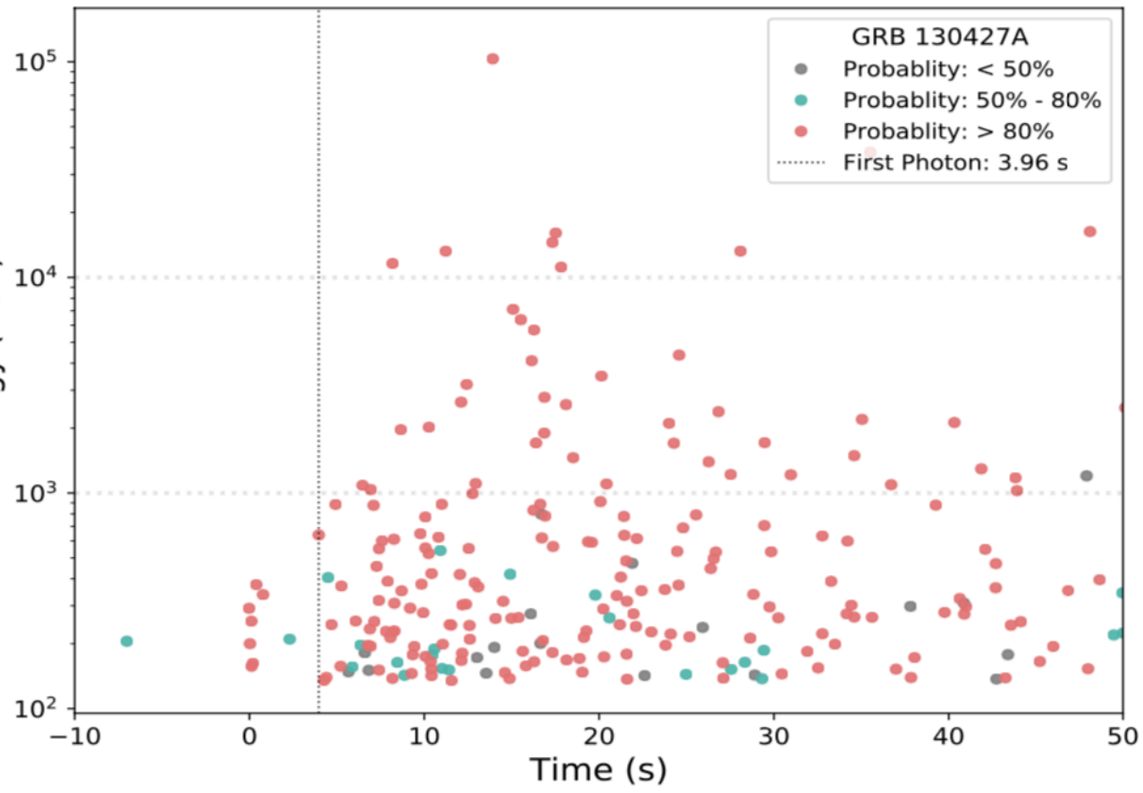

Figure 20. Upper panel: properties of the prompt emission phase of GRB 130427A. The redshift for this burst is 0.34 (Levan et al. 2013). The light-curve consists several spikes, the isotropic energy in the first one is $(0.65 \pm 0.17) \times 10^{52}$ erg. The total energy is 1.4×10^{54} erg. Lower panel: the arrival time of each Fermi-LAT photon of energy > 100 MeV. The first photon belonging to the UPE arrives at 3.96 s. The onset of the GeV radiation almost coincides with the onset of the UPE. The detailed information for each episode, as well as the GeV and afterglow emissions, see Section 6 and Table 1, which include the typical starting time, the duration, the isotropic energy, and the preferred model.

See Liang, L., et al. (2019), arXiv: 1910.12615

Self-Similarities and Power-laws in the Time-resolved Spectra of GRB 190114C, GRB 130427A, GRB 160509A, and GRB 160625B

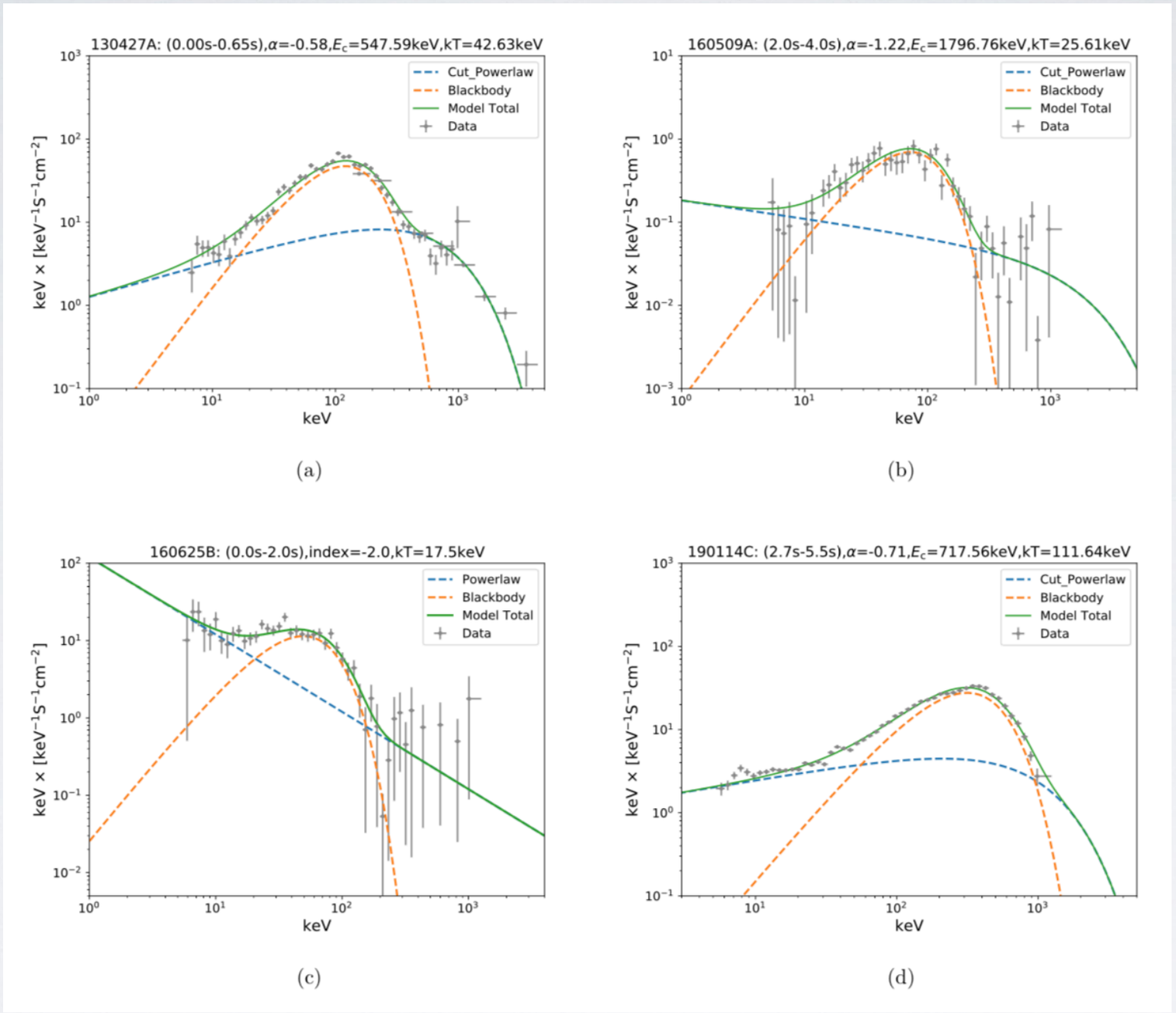

The spectrum of the shock breakout (Episode I) for all our four sources can be fitted by a CPL or PL (synchrotron) components plus a blackbody (thermal) component.

See Liang, L., et al. (2019), arXiv: 1910.12615

Self-Similarities and Power-laws in the Time-resolved Spectra of GRB 190114C, GRB 130427A, GRB 160509A, and GRB 160625B

Table 1. Parameters of the thermal shock breakout for the four precursors of the selected BdHNe I, details in the companion paper Li et al., (2019). In the first column the GRB name. In the second column and following ones the duration, respectively, in the rest frame and in the laboratory frame, the flux, the temperature, and the energy of the shock breakout E_{sh}. In the sixth column the GRB E_{iso}, well above the minimum energy of 10^{52} erg for the BdHN I and in the seventh column the redshift. In the last column, the evidence of the SN in GRB 190114C and GRB 130427A, directly derived from the optical observations. In the case of GRB 160509A and GRB 160625B the evidence of the SN is indirectly inferred from the mass and the spin of the νNS in the afterglows (see R. Ruffini, M. Karlica, et al. 2019, in preparation). Particularly significant is the proportionality of the E_{sh} to the rotational energy of the co-rotating CO_{core} in the binary system of period $P \sim 4$ min. For the spectral analysis technique see caption of Table 2.

GRB	$t_1 \sim t_2$	Duration[a]	Flux	E_{sh}	E_{iso}	Temperature	redshift	Reference
	(s)	(s)	(erg cm^{-2} s^{-1})	(10^{52} erg)	(erg)	(keV)		
	(Observation)	(Rest)		(Shockwave Breakout)	(Total)	(Rest)		(For SN)
190114C	1.12∼1.68	0.39	$1.06^{+0.20}_{-0.20}(10^{-4})$	$2.82^{+0.13}_{-0.13}$	$(2.48\pm0.20)\times10^{53}$	$27.4^{+45.4}_{-25.6}$	0.424	Melandri et al. (2019)
130427A	0.0∼2.6	1.94	$2.14^{+0.28}_{-0.26}(10^{-5})$	$0.65^{+0.17}_{-0.17}$	$\sim1.40\times10^{54}$	$44.9^{+1.5}_{-1.5}$	0.3399	Xu et al. (2013)
160509A	2.0∼4.0	0.92	$1.82^{+1.23}_{-0.76}(10^{-6})$	$1.47^{+0.6}_{-0.6}$	$\sim1.06\times10^{54}$	$25.6^{+4.8}_{-4.7}$	1.17	Tam et al. (2017)
160625B	-1.0∼2.0	1.25	$6.8^{+1.6}_{-1.6}(10^{-7})$	$1.09^{+0.2}_{-0.2}$	$\sim3.00\times10^{54}$	$36.8^{+1.9}_{-1.9}$	1.406	Afterglow

Table 1 summarize the parameters of the thermal νNν-rise (Episode I) for our four sources.

See Liang, L., et al. (2019), arXiv: 1910.12615

Self-Similarities and Power-laws in the Time-resolved Spectra of GRB 190114C, GRB 130427A, GRB 160509A, and GRB 160625B

5 successive time iterations for UPE (Episode II) phase in GRB 160625B

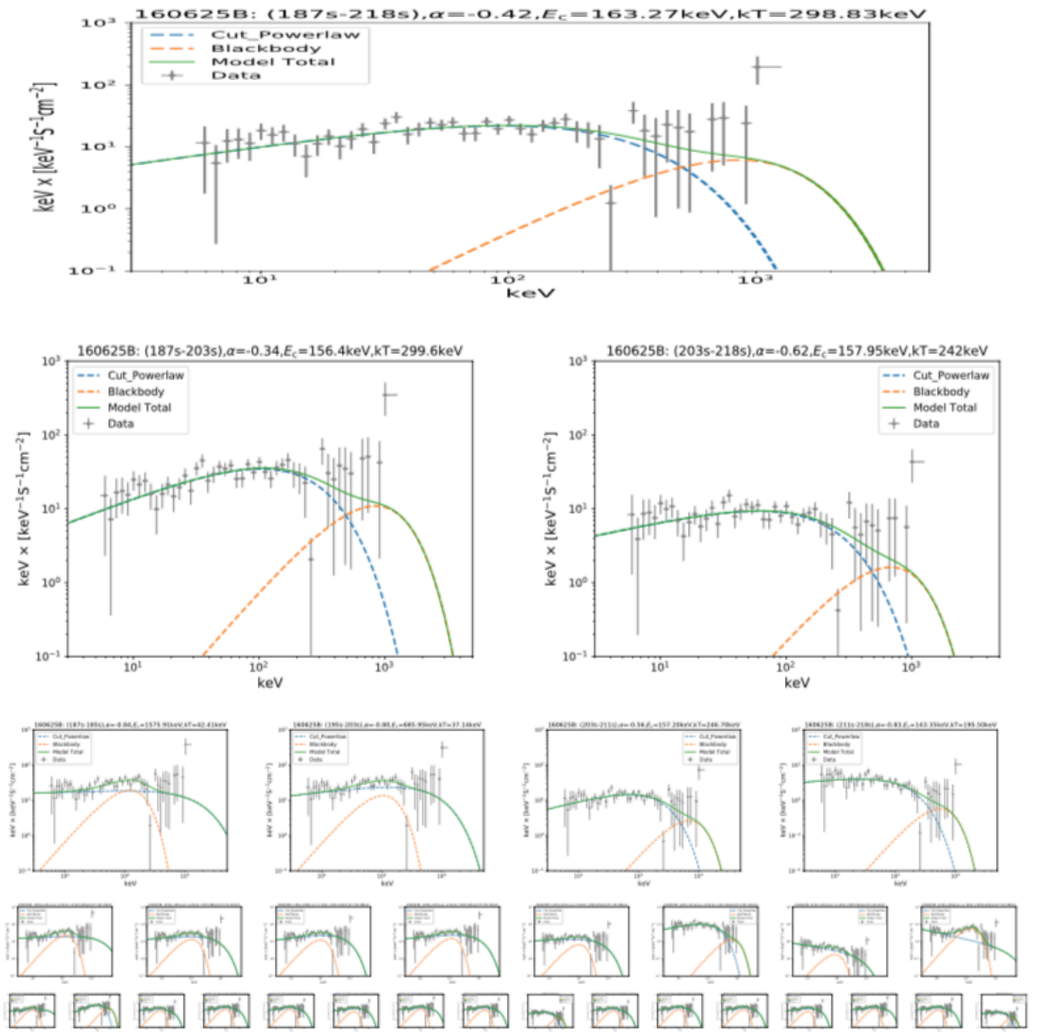

Figure 6. Upper panel: the spectral analysis for the time interval from $t_{\rm rf} = 64.50$ s to $t_{\rm rf} = 79.85$ s. We find the CPL+BB model is the preferred one as compared to all the other models. The best-fit of the power-law index and the cut-off energy of the CPL component are, respectively, $\alpha = -0.42^{+0.01}_{-0.01}$ and $E_c = 163.3^{+2.0}_{-1.9}$, the temperature of the BB component, $kT = 719.0^{+2.3}_{-2.3}$, the DIC with the values of -2937, the BB flux, $F_{\rm BB} = 22.49^{+3.21}_{-2.65}$ and the total flux (CPL+BB), $F_{\rm Total} = 2.85^{+0.07}_{-0.07} \times 10^{-5}$ erg cm^{-2} s^{-1} are reported in Table. 1. The BB to total flux ratio, $F_{\rm BB}/F_{\rm Total} = 0.5$ and the isotropic energy of this time interval, $E_{\rm iso} = 4.25 \times 10^{54}$ erg. The second, third, and bottom panels are the same as the upper panel, but time interval is divided into two equal parts (top line), four equal parts (second line), eight equal parts (third line), and sixteen equal parts (bottom line), respectively.

Table 1. Results of the time-resolved spectral fits of GRB 160625B (CPL+BB model) from the $t_{\rm rf} = 77.72$ s to $t_{\rm rf} = 90.61$ s. This table reports: the time intervals both in rest-frame and observer frame, the power-law index, cut-off energy, temperature, Δ DIC, BB flux, total flux, the BB to total flux ratio, $F_{\rm BB}/F_{\rm Total}$ and finally the isotropic energy. To select the best model from two different given models, we adopt the deviance information criterion (DIC, Yu et al. 2018; Li 2019), defined as DIC=-2log[p(data$|\,\hat{\theta}$)]+2$p_{\rm DIC}$, where $\hat{\theta}$ is the posterior mean of the parameters, and $p_{\rm DIC}$ is the effective number of parameters. The preferred model is the model with the lowest DIC score. Here we define ΔDIC=(CPL+BB)-CPL, if ΔDIC is negative, indicating the CPL+BB is better. After comparing the DIC, we find the CPL+BB model is the preferred model than the CPL and other model. The Δ DIC scores are reported in column 6.

$t_1\sim t_2$	$t_1\sim t_2$	α	E_c	kT	ΔDIC	$F_{\rm BB}$	$F_{\rm Total}$	$F_{\rm ratio}$	$E_{\rm Total}$
(s) Obs	(s) Rest		(keV)	(keV) Rest		(10^{-6}) (erg cm^{-2} s^{-1})	(10^{-6}) (erg cm^{-2} s^{-1})		(erg) Rest
(1)	(2)	(3)	(4)	(5)	(6)	(7)	(8)	(9)	(10)
187.00∼218.00	77.72∼90.61	$-0.83^{+0.01}_{-0.01}$	$686.2^{+13.2}_{-13.4}$	$42.5^{+0.5}_{-0.5}$	-2328.2	$2.33^{+0.13}_{-0.11}$	$27.56^{+0.68}_{-0.70}$	$0.08^{+0.01}_{-0.0}$	4.54e+54
187.00∼203.00	77.72∼84.37	$-0.82^{+0.01}_{-0.01}$	$792.5^{+15.2}_{-15.4}$	$44.5^{+0.4}_{-0.4}$	-3275.1	$4.47^{+0.23}_{-0.22}$	$48.59^{+1.19}_{-1.17}$	$0.09^{+0.01}_{-0.01}$	4.13e+54
203.00∼218.00	84.37∼90.61	$-0.94^{+0.02}_{-0.02}$	$463.9^{+23.2}_{-23.2}$	$36.3^{+1.2}_{-1.2}$	-146.8	$0.58^{+0.11}_{-0.09}$	$7.43^{+0.47}_{-0.41}$	$0.08^{+0.02}_{-0.01}$	5.92e+53
187.00∼195.00	77.72∼81.05	$-0.94^{+0.01}_{-0.01}$	$1575.9^{+42.2}_{-42.0}$	$42.4^{+0.4}_{-0.4}$	-3624.6	$5.96^{+6.23}_{-5.65}$	$56.51^{+59.31}_{-53.78}$	$0.11^{+0.16}_{-0.14}$	2.40e+54
195.00∼203.00	81.05∼84.37	$-0.80^{+0.01}_{-0.01}$	$686.0^{+16.1}_{-16.4}$	$37.1^{+0.5}_{-0.5}$	-1604.9	$3.68^{+3.93}_{-3.42}$	$42.08^{+44.83}_{-39.66}$	$0.09^{+0.13}_{-0.12}$	1.79e+54
203.00∼211.00	84.37∼87.70	$-0.89^{+0.02}_{-0.02}$	$461.9^{+21.2}_{-21.2}$	$37.2^{+1.2}_{-1.2}$	-186.0	$1.00^{+0.17}_{-0.13}$	$12.20^{+0.73}_{-0.64}$	$0.08^{+0.01}_{-0.01}$	5.19e+53
211.00∼218.00	87.70∼90.61	$-1.18^{+0.06}_{-0.06}$	$500.1^{+103.0}_{-107.6}$	$28.4^{+2.5}_{-2.4}$	-26.1	$0.18^{+0.09}_{-0.07}$	$2.09^{+0.48}_{-0.34}$	$0.08^{+0.05}_{-0.04}$	7.79e+52
187.00∼191.00	77.72∼79.38	$-0.92^{+0.01}_{-0.01}$	$2129.5^{+53.8}_{-53.9}$	$46.3^{+0.5}_{-0.5}$	-3279.2	$7.64^{+8.07}_{-7.22}$	$78.67^{+82.43}_{-74.75}$	$0.10^{+0.14}_{-0.13}$	1.67e+54
191.00∼195.00	79.38∼81.05	$-0.85^{+0.01}_{-0.01}$	$655.7^{+25.8}_{-25.8}$	$35.5^{+0.7}_{-0.7}$	-815.9	$3.48^{+3.81}_{-3.16}$	$32.74^{+35.99}_{-30.08}$	$0.11^{+0.16}_{-0.14}$	6.96e+53
195.00∼199.00	81.05∼82.71	$-0.78^{+0.01}_{-0.01}$	$565.3^{+19.2}_{-19.1}$	$34.5^{+0.8}_{-0.8}$	-667.3	$3.10^{+3.43}_{-2.76}$	$34.50^{+37.73}_{-31.35}$	$0.09^{+0.14}_{-0.11}$	7.34e+53
199.00∼203.00	82.71∼84.37	$-0.82^{+0.01}_{-0.01}$	$815.0^{+27.8}_{-27.6}$	$39.8^{+0.8}_{-0.8}$	-972.9	$4.39^{+4.81}_{-3.99}$	$50.51^{+54.58}_{-46.66}$	$0.09^{+0.13}_{-0.11}$	1.07e+54
203.00∼207.00	84.37∼86.03	$-0.90^{+0.02}_{-0.02}$	$566.6^{+32.5}_{-32.9}$	$35.6^{+1.1}_{-1.1}$	-217.0	$1.72^{+1.98}_{-1.49}$	$17.93^{+20.44}_{-15.73}$	$0.10^{+0.16}_{-0.12}$	3.81e+53
207.00∼211.00	86.03∼87.70	$-0.98^{+0.04}_{-0.04}$	$391.2^{+39.2}_{-39.0}$	$33.1^{+1.8}_{-1.8}$	-52.0	$0.61^{+0.20}_{-0.16}$	$6.39^{+0.82}_{-0.66}$	$0.10^{+0.03}_{-0.03}$	1.36e+53
211.00∼215.00	87.70∼89.36	$-1.26^{+0.07}_{-0.07}$	$663.5^{+197.3}_{-205.4}$	$29.1^{+1.8}_{-1.8}$	-19.3	$0.37^{+0.49}_{-0.26}$	$2.85^{+4.45}_{-1.95}$	$0.13^{+0.26}_{-0.13}$	6.06e+52
215.00∼218.00	89.36∼90.61	$-1.38^{+0.39}_{-0.20}$	$3534.3^{+4122.1}_{-3377.8}$	$52.5^{+40.8}_{-28.8}$	-5297.1	$0.16^{+0.80}_{-0.01}$	$1.38^{+53.13}_{-0.45}$	$0.11^{+4.46}_{-0.04}$	2.20e+52
187.00∼189.00	77.72∼78.55	$-0.90^{+0.01}_{-0.01}$	$2774.8^{+101.8}_{-100.9}$	$51.3^{+1.0}_{-1.0}$	-1463.5	$6.21^{+6.82}_{-5.67}$	$68.14^{+73.31}_{-62.60}$	$0.09^{+0.14}_{-0.12}$	7.25e+53
189.00∼191.00	78.55∼79.38	$-0.75^{+0.01}_{-0.02}$	$687.2^{+35.1}_{-13.7}$	$91.2^{+20.9}_{-24.2}$	-2214.8	$3.84^{+0.43}_{-0.48}$	$76.56^{+14.03}_{-4.78}$	$0.05^{+0.01}_{-0.01}$	8.14e+53
191.00∼193.00	79.38∼80.22	$-0.91^{+0.02}_{-0.02}$	$637.9^{+46.0}_{-46.4}$	$33.6^{+0.9}_{-0.9}$	-294.8	$2.77^{+3.18}_{-2.42}$	$23.38^{+27.20}_{-20.28}$	$0.12^{+0.19}_{-0.15}$	2.49e+53
193.00∼195.00	80.22∼81.05	$-0.80^{+0.02}_{-0.02}$	$654.7^{+29.1}_{-29.3}$	$36.8^{+0.9}_{-0.9}$	-513.6	$4.26^{+4.79}_{-3.75}$	$42.42^{+47.55}_{-37.55}$	$0.10^{+0.16}_{-0.13}$	4.51e+53
195.00∼197.00	81.05∼81.88	$-0.81^{+0.02}_{-0.02}$	$607.5^{+28.4}_{-28.6}$	$36.2^{+0.9}_{-0.9}$	-474.3	$4.20^{+4.77}_{-3.76}$	$38.53^{+43.68}_{-34.17}$	$0.11^{+0.17}_{-0.14}$	4.10e+53
197.00∼199.00	81.88∼82.71	$-0.76^{+0.02}_{-0.02}$	$526.8^{+24.2}_{-24.2}$	$31.4^{+1.3}_{-1.3}$	-222.2	$2.04^{+2.48}_{-1.65}$	$30.87^{+35.17}_{-27.36}$	$0.07^{+0.11}_{-0.08}$	3.28e+53
199.00∼201.00	82.71∼83.54	$-0.85^{+0.02}_{-0.02}$	$1042.4^{+58.7}_{-58.1}$	$43.6^{+1.1}_{-1.1}$	-581.4	$5.63^{+6.30}_{-4.95}$	$61.05^{+69.06}_{-53.83}$	$0.09^{+0.15}_{-0.11}$	6.49e+53
201.00∼203.00	83.54∼84.37	$-0.76^{+0.02}_{-0.02}$	$573.5^{+22.2}_{-22.5}$	$40.5^{+1.4}_{-1.3}$	-282.6	$3.17^{+0.56}_{-0.52}$	$42.42^{+2.12}_{-2.38}$	$0.07^{+0.01}_{-0.01}$	4.51e+53
203.00∼205.00	84.37∼85.20	$-0.84^{+0.02}_{-0.02}$	$521.4^{+31.0}_{-30.7}$	$39.9^{+2.0}_{-2.0}$	-88.3	$1.51^{+0.43}_{-0.34}$	$21.61^{+1.84}_{-1.67}$	$0.07^{+0.02}_{-0.02}$	2.30e+53
205.00∼207.00	85.20∼86.03	$-0.82^{+0.03}_{-0.03}$	$415.0^{+31.4}_{-31.4}$	$37.2^{+2.1}_{-2.1}$	-71.3	$1.26^{+0.40}_{-0.31}$	$14.52^{+1.60}_{-1.31}$	$0.09^{+0.03}_{-0.02}$	1.54e+53
207.00∼209.00	86.03∼86.87	$-1.00^{+0.05}_{-0.05}$	$425.7^{+55.3}_{-55.3}$	$34.7^{+2.0}_{-2.0}$	-44.8	$0.87^{+0.30}_{-0.22}$	$7.44^{+1.23}_{-0.97}$	$0.12^{+0.04}_{-0.03}$	7.91e+52
209.00∼211.00	86.87∼87.70	$-0.95^{+0.06}_{-0.06}$	$354.2^{+49.3}_{-50.3}$	$30.0^{+3.5}_{-3.5}$	-20.3	$0.34^{+0.24}_{-0.17}$	$5.42^{+1.13}_{-0.84}$	$0.06^{+0.05}_{-0.03}$	5.77e+52
211.00∼213.00	87.70∼88.53	$-1.07^{+0.06}_{-0.06}$	$427.6^{+82.5}_{-82.9}$	$26.4^{+2.7}_{-2.7}$	-27.2	$0.33^{+0.20}_{-0.14}$	$4.03^{+0.99}_{-0.77}$	$0.08^{+0.05}_{-0.04}$	4.29e+52
213.00∼215.00	88.53∼89.36	$-1.40^{+0.13}_{-0.13}$	$998.0^{+654.7}_{-576.7}$	$31.9^{+4.3}_{-3.4}$	-21.6	$0.23^{+0.17}_{-0.12}$	$1.68^{+0.88}_{-0.56}$	$0.14^{+0.12}_{-0.08}$	1.78e+52
215.00∼217.00	89.36∼90.19	$-1.16^{+0.11}_{-0.11}$	$527.4^{+207.6}_{-225.0}$	$28.5^{+8.7}_{-14.4}$	-91.8	$0.03^{+0.41}_{-0.03}$	$1.24^{+1.25}_{-0.41}$	$0.02^{+0.33}_{-0.02}$	1.32e+52
217.00∼219.00	90.19∼91.02	$-1.43^{+0.49}_{-0.28}$	$3502.1^{+4174.8}_{-3354.0}$	$44.9^{+3.4}_{-16.0}$	-876.2	$0.23^{+0.61}_{-0.06}$	$1.03^{+45.16}_{-0.36}$	$0.22^{+9.63}_{-0.09}$	1.10e+52

See Liang, L., et al. (2019), arXiv: 1910.12615

Self-Similarities and Power-laws in the Time-resolved Spectra of GRB 190114C, GRB 130427A, GRB 160509A, and GRB 160625B

5 successive time iterations for UPE (Episode II) in GRB 160509A

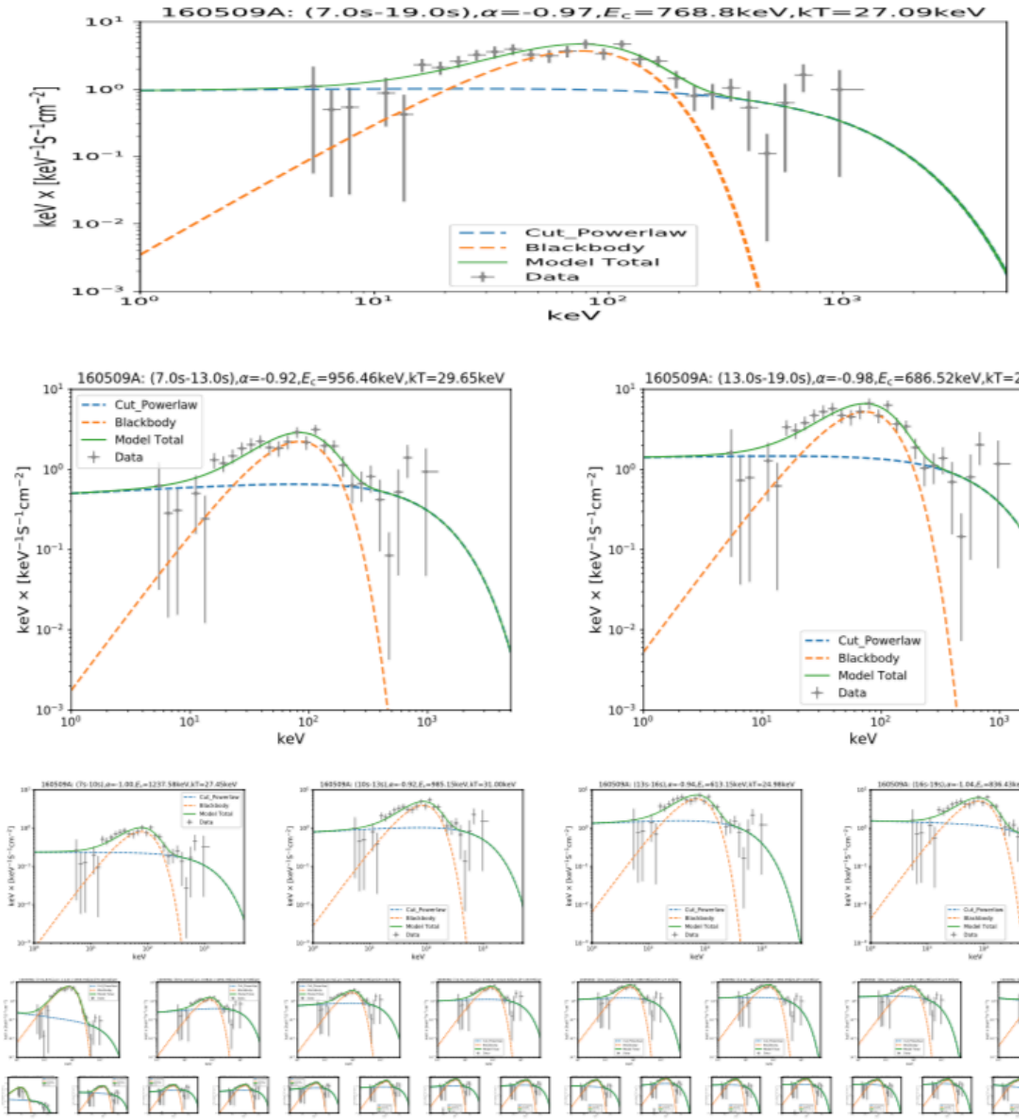

Figure 10. Upper panel: the spectral analysis for the time interval from $t_{\rm rf} = 3.23$ s to $t_{\rm rf} = 8.76$ s. We find the CPL+BB model is the preferred one as compared to all the other models. The best-fit of the power-law index and the cut-off energy of the CPL component are, respectively, $\alpha = -0.97^{+0.01}_{-0.01}$ and $E_c = 768.8^{+28.4}_{-28.8}$, the temperature of the BB component, $kT = 27.1^{+0.6}_{-0.6}$, the Δ DIC with the values of -658, the BB flux, $F_{\rm BB} = 0.73^{+0.09}_{-0.08}$ and the total flux (CPL+BB), $F_{\rm Total} = 14.01^{+0.79}_{-0.72} \times 10^{-6}$ (erg cm^{-2} s^{-1}) are reported in Table. 2. The BB to total flux ratio, $F_{\rm BB}/F_{\rm Total} = 0.05$ and the isotropic energy of this time interval, $E_{\rm iso} = 6.30 \times 10^{53}$ erg. The second, third, and bottom panels are the same as the upper panel, but time interval is divided into two equal parts (top line), four equal parts (second line), eight equal parts (third line), and sixteen equal parts (bottom line), respectively.

Table 2. Results of the time-resolved spectral fits of GRB 160509A (CPL+BB model) from the $t_{\rm rf} = 3.23$ s to $t_{\rm rf} = 8.76$ s. This table reports: the time intervals both in rest-frame and observer frame, the power-law index, cut-off energy, temperature, Δ DIC, BB flux, total flux, the BB to total flux ratio, $F_{\rm BB}/F_{\rm Total}$ and finally the isotropic energy. The $F_{\rm BB}/F_{\rm Total}$ remains almost constant in each sample. To select the best model from two different given models, we adopt the deviance information criterion (DIC, Yu et al. 2018; Li 2019) in this paper, defined as DIC=-2log$[p(\text{data}|\hat{\theta})]$+2$p_{\rm DIC}$, where $\hat{\theta}$ is the posterior mean of the parameters, and $p_{\rm DIC}$ is the effective number of parameters. The preferred model is the model with the lowest DIC score. Here we define ΔDIC=(CPL+BB)-CPL, if ΔDIC is negative, indicating the CPL+BB is better. After comparing the DIC, we find the CPL+BB model is the preferred model than the CPL and other model.

t_1~t_2 (s) Obs	t_1~t_2 (s) Rest	α	E_c (keV)	kT	ΔDIC	$F_{\rm BB}$ (10^{-6}) (erg cm^{-2} s^{-1})	$F_{\rm Total}$ (10^{-6}) (erg cm^{-2} s^{-1})	$F_{\rm ratio}$	$E_{\rm Total}$ (erg)
(1)	(2)	(3)	(4)	(5)	(6)	(7)	(8)	(9)	(10)
7.00~19.00	3.23~8.76	$-0.97^{+0.01}_{-0.01}$	$768.8^{+28.4}_{-28.8}$	$27.1^{+0.6}_{-0.6}$	-658.0	$0.73^{+0.09}_{-0.08}$	$14.01^{+0.79}_{-0.72}$	$0.05^{+0.01}_{-0.01}$	6.30e+53
7.00~13.00	3.23~5.99	$-0.92^{+0.02}_{-0.02}$	$956.5^{+71.8}_{-71.1}$	$29.6^{+1.2}_{-1.2}$	-194.6	$0.49^{+0.11}_{-0.10}$	$10.80^{+1.19}_{-1.08}$	$0.04^{+0.01}_{-0.01}$	2.43e+53
13.00~19.00	5.99~8.76	$-0.98^{+0.01}_{-0.01}$	$686.5^{+27.1}_{-27.2}$	$26.1^{+0.7}_{-0.7}$	-495.0	$0.99^{+0.15}_{-0.13}$	$17.65^{+1.03}_{-1.09}$	$0.06^{+0.01}_{-0.01}$	3.97e+53
7.00~10.00	3.23~4.61	$-1.00^{+0.04}_{-0.04}$	$1237.6^{+241.5}_{-247.0}$	$27.4^{+3.0}_{-3.1}$	-30.2	$0.14^{+0.12}_{-0.07}$	$4.69^{+1.55}_{-1.09}$	$0.03^{+0.03}_{-0.02}$	5.27e+52
10.00~13.00	4.61~5.99	$-0.92^{+0.02}_{-0.02}$	$985.1^{+75.6}_{-75.7}$	$31.0^{+1.4}_{-1.4}$	-202.9	$0.86^{+0.23}_{-0.17}$	$17.69^{+2.31}_{-1.82}$	$0.05^{+0.01}_{-0.01}$	1.99e+53
13.00~16.00	5.99~7.37	$-0.94^{+0.02}_{-0.02}$	$613.1^{+31.0}_{-30.8}$	$25.0^{+0.8}_{-0.8}$	-305.8	$1.05^{+0.19}_{-0.18}$	$17.02^{+1.37}_{-1.21}$	$0.06^{+0.01}_{-0.01}$	1.91e+53
13.00~16.00	5.99~7.37	$-0.94^{+0.02}_{-0.02}$	$612.8^{+30.7}_{-31.0}$	$25.0^{+0.8}_{-0.8}$	-305.8	$1.05^{+0.19}_{-0.16}$	$16.96^{+1.30}_{-1.29}$	$0.06^{+0.01}_{-0.01}$	1.91e+53
16.00~19.00	7.37~8.76	$-1.04^{+0.02}_{-0.02}$	$836.4^{+59.4}_{-61.8}$	$28.4^{+1.2}_{-1.2}$	-218.1	$1.04^{+0.25}_{-0.21}$	$18.84^{+1.84}_{-1.65}$	$0.06^{+0.01}_{-0.01}$	2.12e+53
7.00~8.50	3.23~3.92	$-1.20^{+0.10}_{-0.10}$	$1363.9^{+973.5}_{-781.1}$	$26.0^{+11.0}_{-16.4}$	-2831.7	$0.06^{+1.00}_{-0.06}$	$2.18^{+3.59}_{-1.00}$	$0.03^{+0.46}_{-0.03}$	1.23e+52
8.50~10.00	3.92~4.61	$-0.88^{+0.05}_{-0.05}$	$1091.4^{+189.6}_{-193.4}$	$27.8^{+3.4}_{-3.3}$	-30.2	$0.22^{+0.18}_{-0.10}$	$7.25^{+2.46}_{-1.77}$	$0.03^{+0.03}_{-0.02}$	4.08e+52
8.50~10.00	3.92~4.61	$-0.88^{+0.05}_{-0.04}$	$1088.3^{+184.9}_{-187.9}$	$28.0^{+3.4}_{-3.4}$	-30.0	$0.23^{+0.19}_{-0.12}$	$7.19^{+2.33}_{-1.64}$	$0.03^{+0.03}_{-0.02}$	4.04e+52
10.00~11.50	4.61~5.30	$-0.91^{+0.04}_{-0.04}$	$994.6^{+142.5}_{-144.6}$	$34.2^{+2.6}_{-2.6}$	-64.0	$0.69^{+0.32}_{-0.21}$	$13.71^{+3.26}_{-2.43}$	$0.05^{+0.03}_{-0.02}$	7.70e+52
11.50~13.00	5.30~5.99	$-0.94^{+0.02}_{-0.02}$	$1022.5^{+89.6}_{-89.2}$	$29.9^{+1.4}_{-1.4}$	-155.8	$1.11^{+0.30}_{-0.22}$	$22.32^{+3.10}_{-2.60}$	$0.05^{+0.02}_{-0.01}$	1.25e+53
13.00~14.50	5.99~6.68	$-0.93^{+0.02}_{-0.02}$	$696.5^{+57.8}_{-57.6}$	$27.0^{+1.3}_{-1.3}$	-159.7	$1.12^{+0.31}_{-0.25}$	$18.38^{+2.44}_{-2.17}$	$0.06^{+0.02}_{-0.02}$	1.03e+53
14.50~16.00	6.68~7.37	$-0.96^{+0.02}_{-0.02}$	$560.4^{+35.9}_{-35.7}$	$23.6^{+1.1}_{-1.1}$	-159.2	$1.02^{+0.27}_{-0.23}$	$16.03^{+1.68}_{-1.62}$	$0.06^{+0.02}_{-0.02}$	9.01e+52
16.00~17.50	7.37~8.06	$-0.97^{+0.02}_{-0.02}$	$583.3^{+41.6}_{-42.1}$	$27.3^{+1.7}_{-1.7}$	-91.1	$0.93^{+0.40}_{-0.26}$	$18.48^{+2.06}_{-1.75}$	$0.05^{+0.02}_{-0.01}$	1.04e+53
17.50~19.00	8.06~8.76	$-1.14^{+0.02}_{-0.02}$	$1666.7^{+220.4}_{-215.5}$	$30.3^{+1.6}_{-1.6}$	-153.3	$1.11^{+0.35}_{-0.26}$	$21.74^{+3.58}_{-2.76}$	$0.05^{+0.02}_{-0.01}$	1.22e+53
7.00~7.75	3.23~3.57	$-1.26^{+0.15}_{-0.13}$	$396.4^{+153.8}_{-140.3}$	$17.6^{+8.7}_{-6.8}$	-17.5	$0.02^{+0.16}_{-0.01}$	$0.74^{+0.69}_{-0.32}$	$0.02^{+0.22}_{-0.02}$	2.07e+51
7.75~8.50	3.57~3.92	$-1.06^{+0.09}_{-0.09}$	$1256.7^{+489.8}_{-515.8}$	$23.9^{+6.2}_{-5.3}$	-21.8	$0.13^{+0.27}_{-0.10}$	$3.06^{+2.59}_{-1.22}$	$0.04^{+0.10}_{-0.04}$	8.60e+51
8.50~9.25	3.92~4.26	$-0.86^{+0.06}_{-0.06}$	$1125.8^{+272.9}_{-264.1}$	$24.6^{+3.9}_{-3.8}$	-19.5	$0.19^{+0.24}_{-0.11}$	$7.27^{+3.56}_{-2.35}$	$0.03^{+0.04}_{-0.02}$	2.04e+52
9.25~10.00	4.26~4.61	$-0.91^{+0.06}_{-0.06}$	$1145.0^{+269.7}_{-284.4}$	$31.0^{+4.9}_{-4.9}$	-21.9	$0.25^{+0.32}_{-0.14}$	$7.52^{+3.93}_{-2.36}$	$0.03^{+0.05}_{-0.02}$	2.11e+52
10.00~10.75	4.61~4.95	$-0.89^{+0.05}_{-0.05}$	$1018.9^{+221.3}_{-221.4}$	$35.7^{+5.0}_{-4.9}$	-27.4	$0.52^{+0.49}_{-0.26}$	$11.54^{+4.46}_{-3.16}$	$0.04^{+0.05}_{-0.03}$	3.24e+52
10.75~11.50	4.95~5.30	$-0.93^{+0.05}_{-0.05}$	$1053.9^{+204.1}_{-207.5}$	$33.9^{+3.2}_{-3.2}$	-47.9	$0.87^{+0.54}_{-0.34}$	$16.25^{+5.69}_{-4.08}$	$0.05^{+0.04}_{-0.02}$	4.57e+52
11.50~12.25	5.30~5.65	$-0.93^{+0.03}_{-0.03}$	$1173.2^{+136.5}_{-135.9}$	$29.6^{+1.7}_{-1.7}$	-120.2	$1.30^{+0.46}_{-0.34}$	$23.42^{+4.74}_{-3.89}$	$0.06^{+0.02}_{-0.02}$	6.58e+52
12.25~13.00	5.65~5.99	$-0.93^{+0.03}_{-0.03}$	$884.5^{+104.1}_{-104.7}$	$29.9^{+2.6}_{-2.7}$	-51.4	$0.87^{+0.51}_{-0.31}$	$21.70^{+4.34}_{-3.63}$	$0.04^{+0.02}_{-0.02}$	6.10e+52
13.00~13.75	5.99~6.34	$-1.03^{+0.03}_{-0.03}$	$1045.1^{+157.7}_{-160.7}$	$28.6^{+2.0}_{-2.1}$	-73.1	$0.98^{+0.44}_{-0.30}$	$17.00^{+3.92}_{-3.06}$	$0.06^{+0.03}_{-0.02}$	4.78e+52
13.75~14.50	6.34~6.68	$-0.87^{+0.03}_{-0.03}$	$571.0^{+48.5}_{-48.8}$	$26.2^{+1.6}_{-1.6}$	-94.7	$1.29^{+0.50}_{-0.33}$	$20.52^{+3.46}_{-2.57}$	$0.06^{+0.03}_{-0.02}$	5.77e+52
14.50~15.25	6.68~7.03	$-0.97^{+0.03}_{-0.03}$	$598.2^{+56.3}_{-57.2}$	$23.6^{+1.5}_{-1.6}$	-75.6	$0.91^{+0.40}_{-0.26}$	$15.50^{+2.42}_{-2.15}$	$0.06^{+0.03}_{-0.02}$	4.36e+52
15.25~16.00	7.03~7.37	$-0.95^{+0.03}_{-0.03}$	$538.8^{+44.3}_{-45.2}$	$23.7^{+1.4}_{-1.4}$	-88.7	$1.11^{+0.42}_{-0.31}$	$16.51^{+2.55}_{-2.02}$	$0.07^{+0.03}_{-0.02}$	4.64e+52
16.00~16.75	7.37~7.72	$-1.02^{+0.03}_{-0.03}$	$630.1^{+73.4}_{-71.9}$	$27.5^{+2.2}_{-2.2}$	-49.4	$0.96^{+0.46}_{-0.32}$	$17.15^{+3.12}_{-2.38}$	$0.06^{+0.03}_{-0.02}$	4.82e+52
16.75~17.50	7.72~8.06	$-0.93^{+0.03}_{-0.03}$	$560.6^{+54.8}_{-54.0}$	$27.2^{+2.6}_{-2.6}$	-48.3	$0.98^{+0.56}_{-0.40}$	$19.97^{+3.00}_{-2.75}$	$0.05^{+0.03}_{-0.02}$	5.61e+52
17.50~18.25	8.06~8.41	$-1.13^{+0.02}_{-0.02}$	$2147.2^{+335.2}_{-327.7}$	$33.0^{+2.4}_{-2.4}$	-94.6	$1.22^{+0.60}_{-0.39}$	$28.85^{+5.60}_{-4.36}$	$0.04^{+0.02}_{-0.01}$	8.11e+52
18.25~19.00	8.41~8.76	$-1.11^{+0.04}_{-0.04}$	$971.3^{+183.5}_{-187.3}$	$26.8^{+2.1}_{-2.1}$	-60.3	$0.91^{+0.43}_{-0.32}$	$14.70^{+4.23}_{-2.90}$	$0.06^{+0.03}_{-0.03}$	4.13e+52

See Liang, L., et al. (2019), arXiv: 1910.12615

Self-Similarities and Power-laws in the Time-resolved Spectra of GRB 190114C, GRB 130427A, GRB 160509A, and GRB 160625B

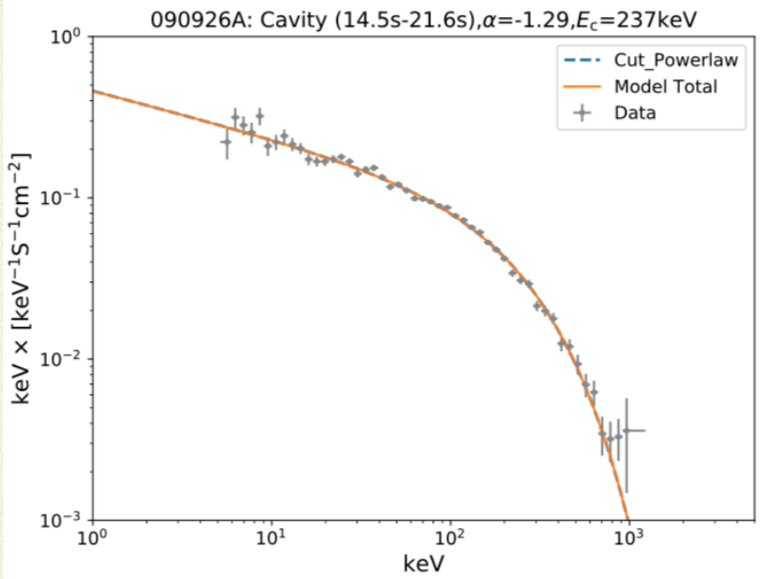

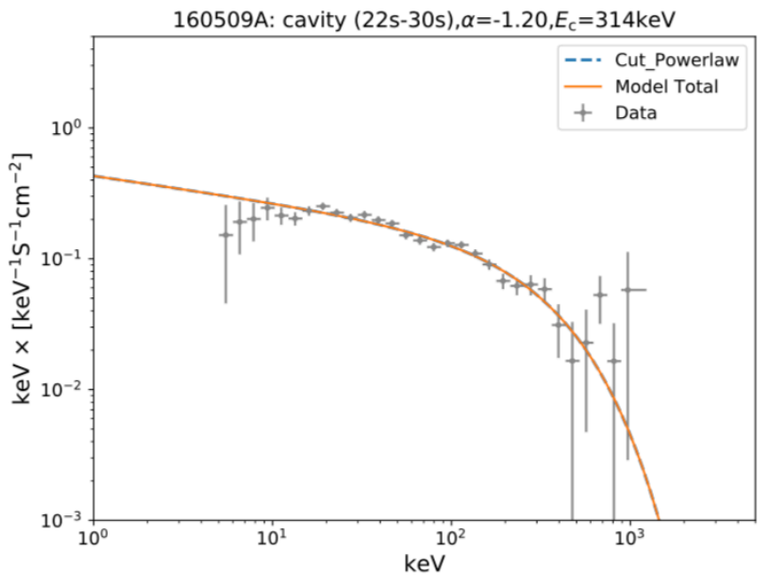

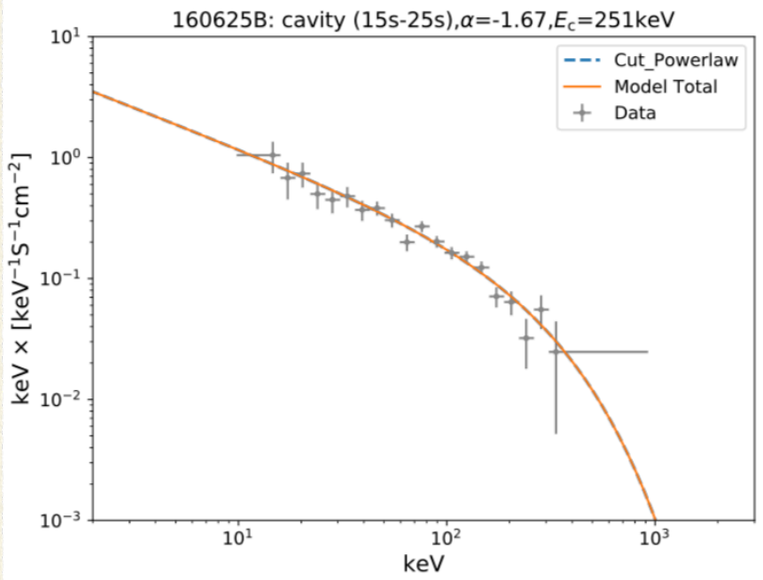

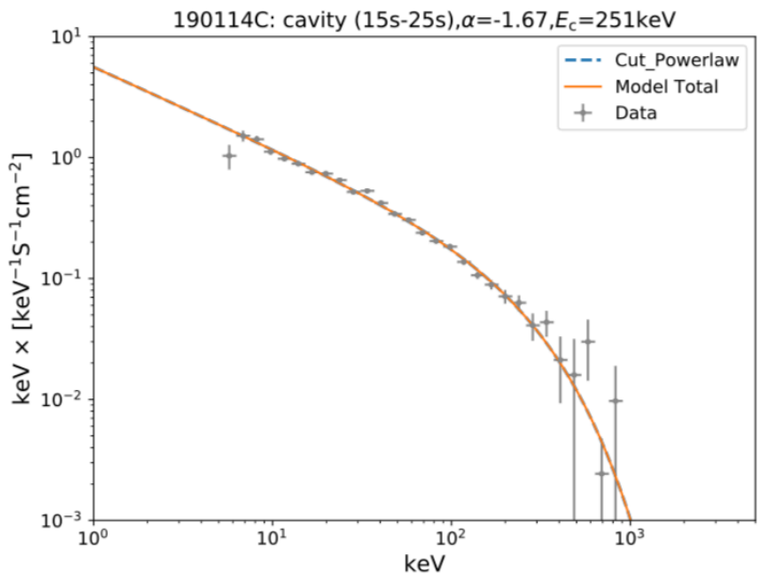

The spectral component of the cavity (episode III) for our four sources can be well fitted by a featureless CPL model.

See Liang, L., et al. (2019), arXiv: 1910.12615

Self-Similarities and Power-laws in the Time-resolved Spectra of GRB 190114C, GRB 130427A, GRB 160509A, and GRB 160625B

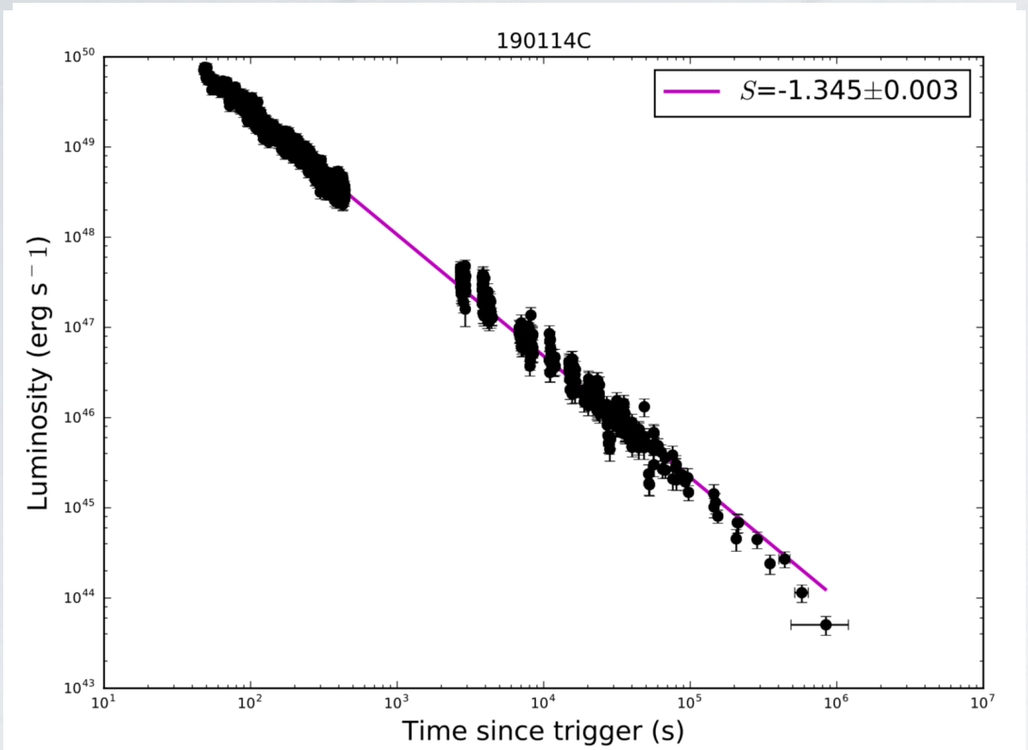

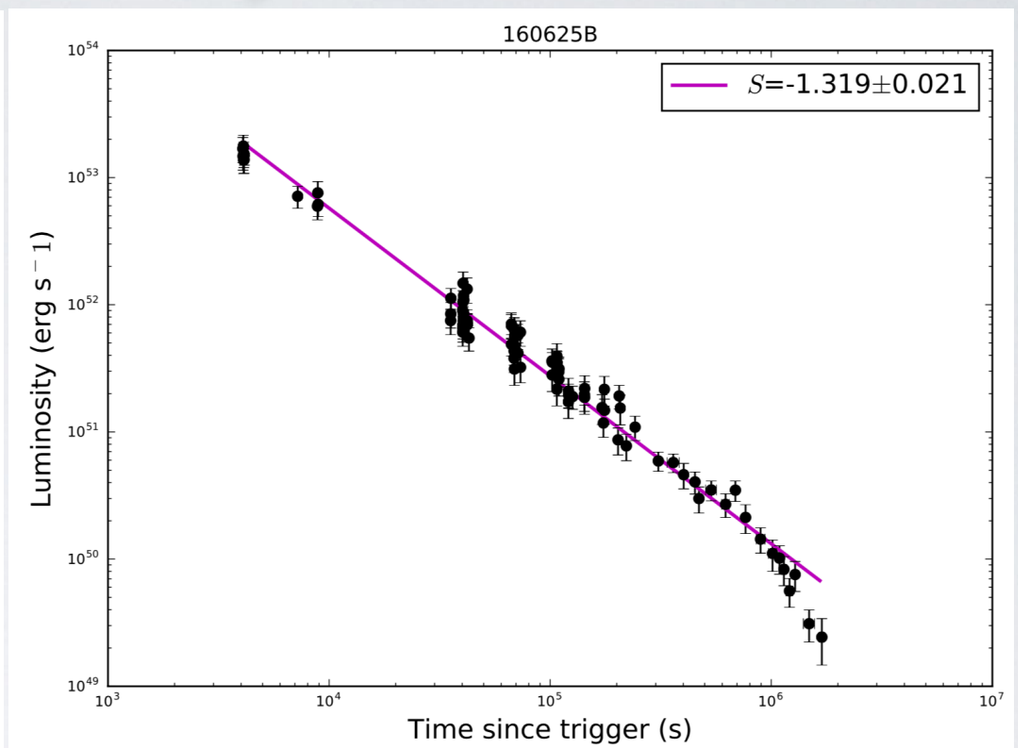

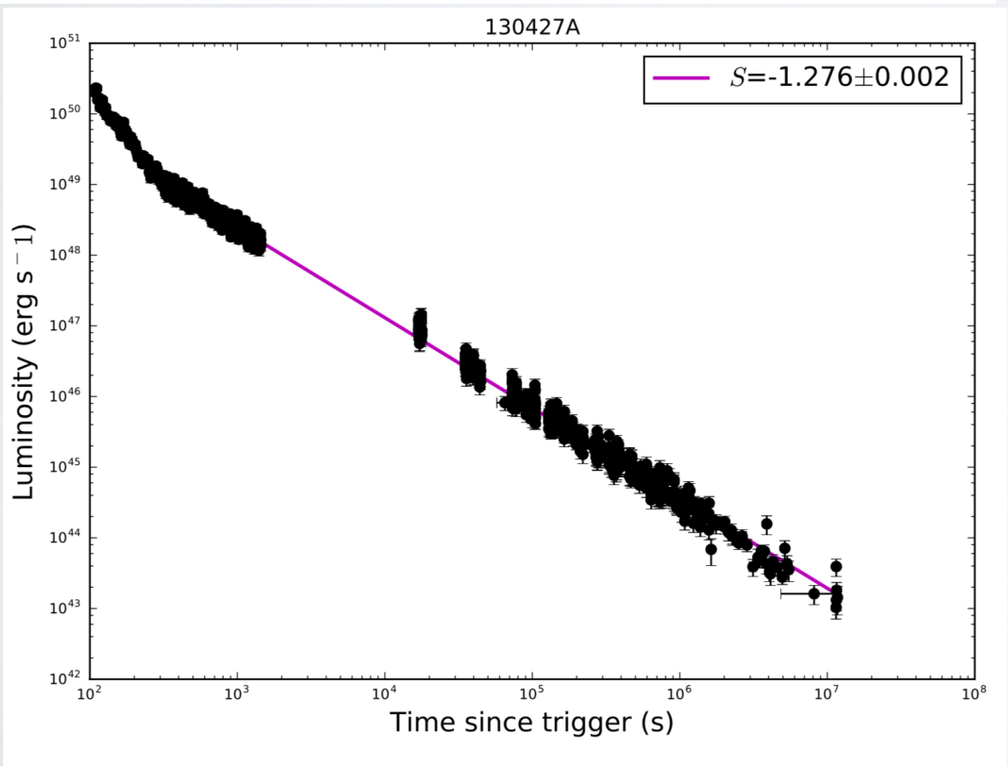

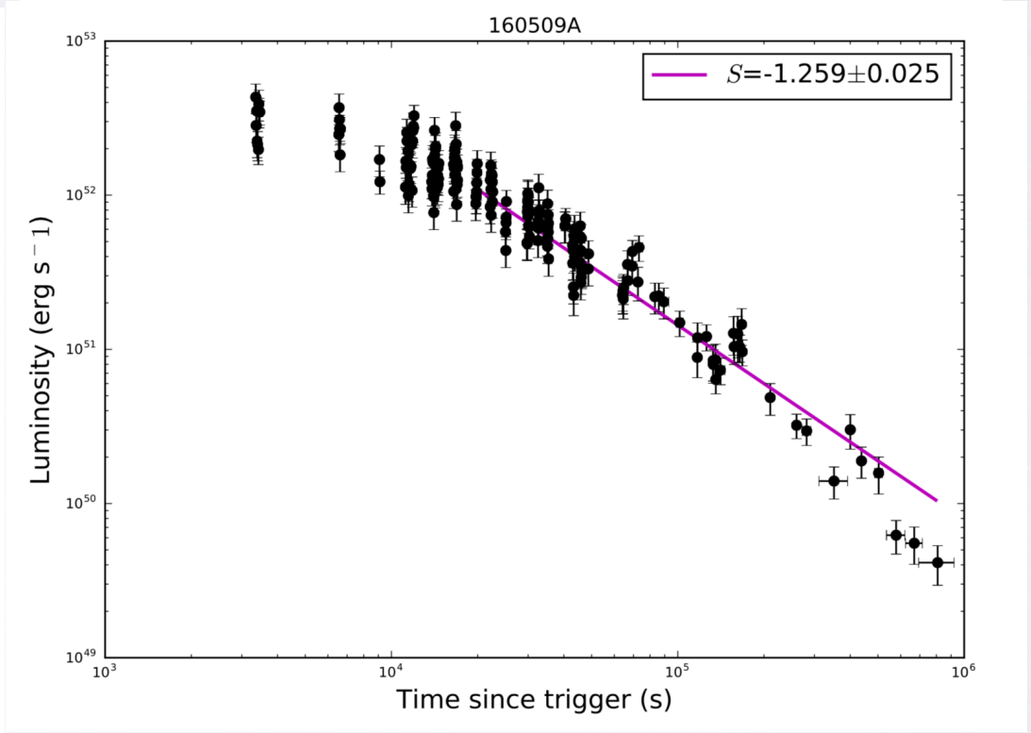

Swfit-XRT light curves for our four sources, all four sources show power-law decays.

See Liang, L., et al. (2019), arXiv: 1910.12615

- *Self-similarity and power-laws in GRB 190114C (arXiv:1904.04162)*
- *Self-Similarities and Power-laws in the Time-resolved Spectra of GRB 190114C, GRB 130427A, GRB 160509A, and GRB 160625B (arXiv:1910.12615)*
- *GRB-SNe association within Binary driven Hypernova (BdHN) (In prep.)*

- *GRB-SNe association within Binary driven Hypernova (BdHN) (In prep.)*

Table 2. Summary of the GRB subclasses. In addition to the subclass name, we report the number of GRBs for each subclass. We recall as well the 'in-state' representing the progenitors and the 'out-state' and the $E_{\rm p,i}$ and $E_{\gamma,\rm iso}$ for each subclass. The GeV emission is indicated in the last column: for long GRBs it appears only in BdHN I and BdHN IV (BH-SN) while, for short bursts, it appears only for S-GRBs. In all sources with GeV emission, it is $\gtrsim 10^{52}$ erg.

Class	Type	Number	In-state	Out-state	$E_{\rm p,\,i}$ (MeV)	$E_{\gamma,\,\rm iso}$ (erg)	$E_{\rm iso,\,Gev}$ (erg)
Binary driven	I	378	CO star–NS	νNS–BH	~0.2–2	$\sim 10^{52}$–10^{54}	$\gtrsim 10^{52}$
hypernova	II	(49)	CO star–NS	νNS–NS	~0.01–0.2	$\sim 10^{50}$–10^{52}	–
(BdHN)	III	(19)	CO star–NS	νNS–NS	~0.01	$\sim 10^{48}$–10^{50}	–
	IV	0	CO star–NS	BH	–	$>10^{54}$	$\gtrsim 10^{53}$
	I	18	NS–NS	MNS	~0.2–2	$\sim 10^{49}$–10^{52}	–
Binary	II	6	NS–NS	BH	~2–8	$\sim 10^{52}$–10^{53}	$\gtrsim 10^{52}$
merger	III	(1)	NS–WD	MNS	~0.2–2	$\sim 10^{49}$–10^{52}	–
(BM)	IV	(1)	WD–WD	NS/MWD	<0.2	$<10^{51}$	–
	V	(0)	NS–BH	Direct BH	$\gtrsim 2$	$>10^{52}$	–

Table is taken from Ruffini, et al. (2021), MNRAS, 504, 5301-5326

GRB-SNe association within Binary driven Hypernova (BdHN)

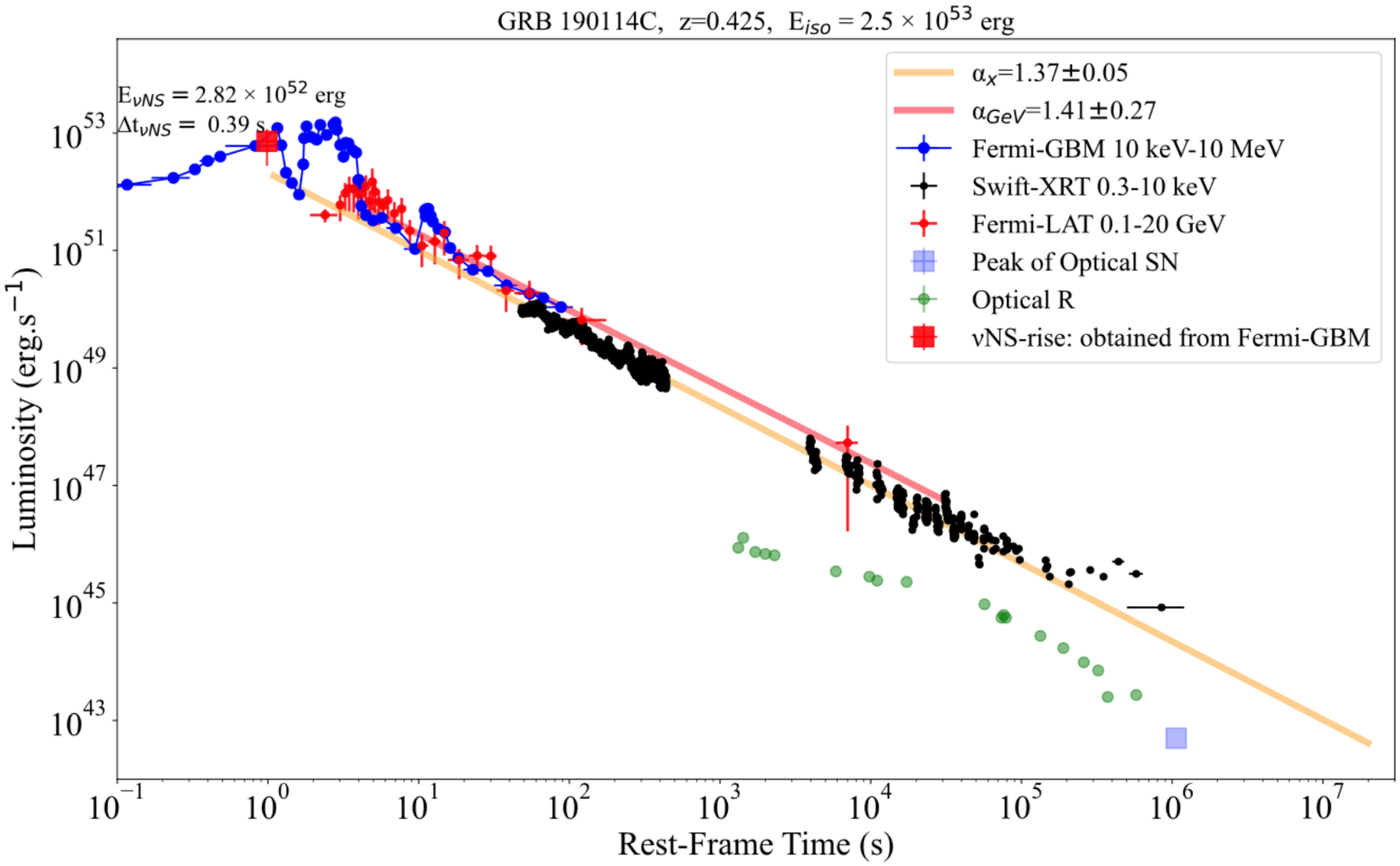

Figure 5. BdHNe I: GRB 190114C. Luminosity light-curves obtained from Fermi-GBM, in 10 keV–10 MeV, Fermi-LAT in 0.1 GeV–10 GeV,Swift-BAT in 15 keV–50 keV, Swift-XRT in 3 keV–10 keV and optical R band. The late X-ray afterglow luminosity of BdHN I GRB 190114C observed by *Swift*-XRT is best fit by a temporal decaying power law of $L_{\rm X} = (2.5 \pm 0.4) \times 10^{53}\ {\rm t}^{1.44\pm0.01}{\rm erg.s}^{-1}$. The light-curve of Fermi–LAT in is fitted by temporal decaying power law of $L_{\rm GeV} = (4.6 \pm 2.9) \times 10^{53}\ {\rm t}^{-1.94\pm0.04}{\rm erg.s}^{-1}$.

BdHNe I: SNe emissions typically are much below their afterglow emissions.

GRB-SNe association within Binary driven Hypernova (BdHN) (In prep.)

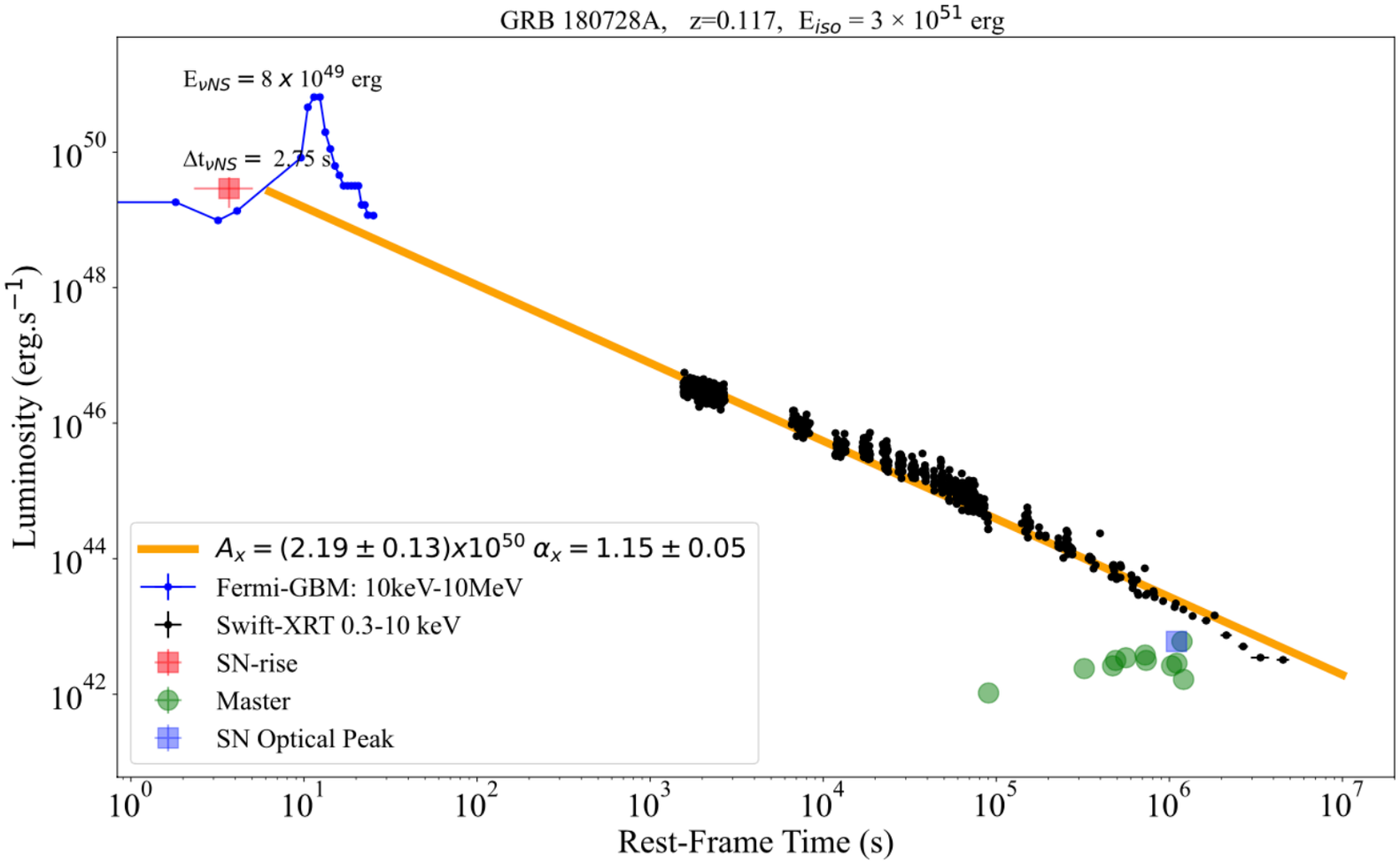

Figure 9. BdHN II: GRB 180728A. Luminosity light-curves obtained from Fermi-GBM, in 10 keV–10 MeV, Swift-BAT in 15 keV–50 keV, Swift-XRT in 3 keV–10 keV and MASTER

BdHNe II: SNe emissions typically are below their afterglow emissions.

GRB-SNe association within Binary driven Hypernova (BdHN) (In prep.)

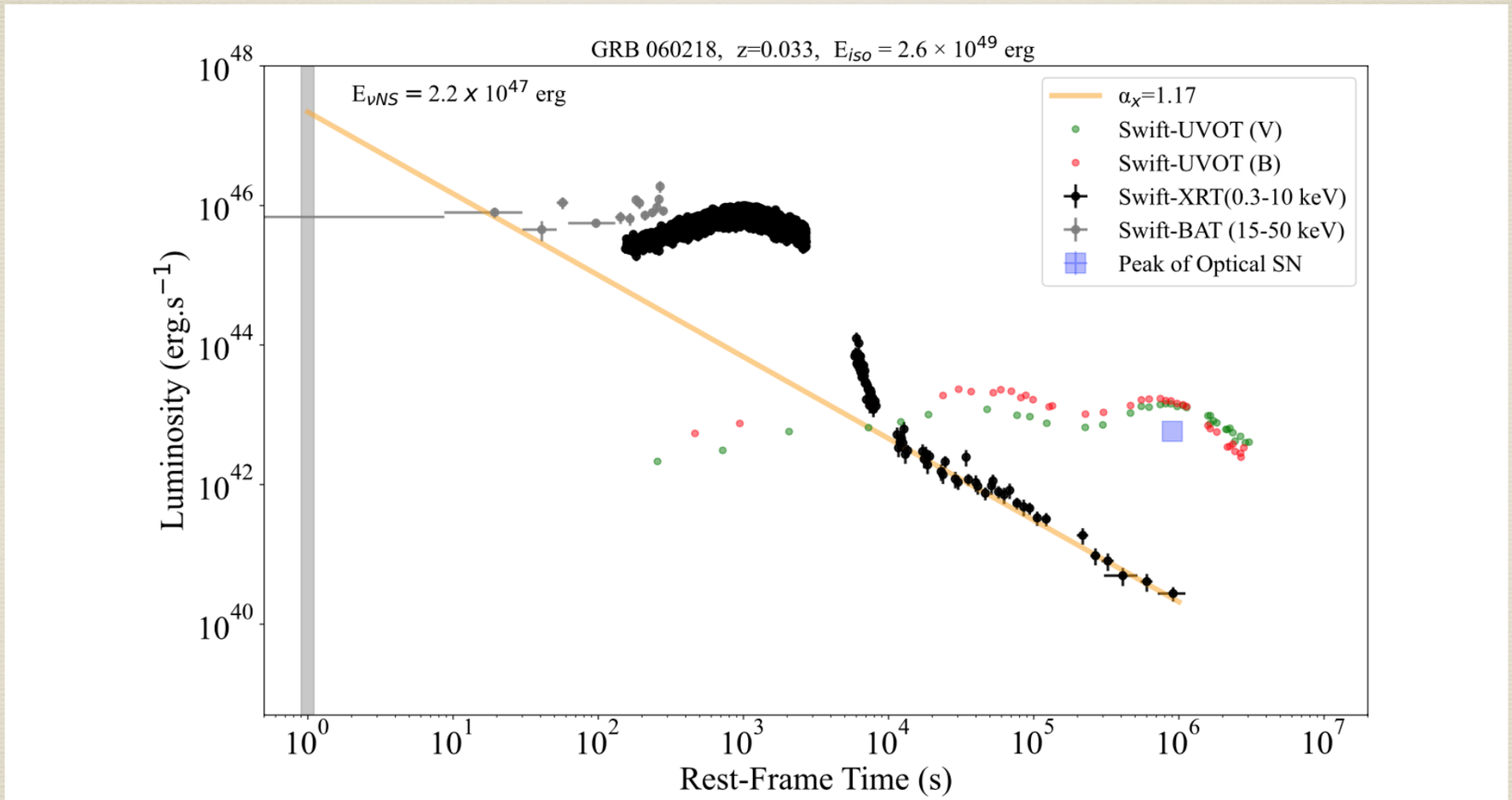

Figure 10. BdHN III: GRB 060218. Luminosity light-curves obtained from Swift-BAT in 15 keV–50 keV, Swift-XRT in 3 keV–10 keV and SWift-UVOT V and B band. After $t_{\rm rf} \sim 10^4$ s it follows a decaying power-law with index $\alpha_X = 1.17 \pm 0.02$ and amplitude of $A_{\rm X} = (2.2 \pm 0.5) \times 10^{47}$erg.s^{-1}.

BdHNe III: SNe emissions typically are above their afterglow emissions.

Conclusions

- *The spectral components of GRB 190114C show three different characteristic for three different Episodes, and the temperature and luminosity in UPE phase for GRB 190114C present a power-laws decay. The observations in GRB 190114C fully consistent with Prof. Ruffini's model.*
- *Such self-similarity and power-laws characteristics are also found in GRB 160625B, GRB 160609A, and GRB 130427A.*
- *We compared the SNe emissions and their afterglow emissions in the GRB-SN association sample, and found that different BdHNe bursts have different behaviors.*

Thanks!